NASA/TP—2013–217917

Behavior of Spinning Space Vehicles with Onboard Liquids, 2nd Edition, Technical Report B8030

Prepared by Carl Hubert
Hubert Astronautics
644 Wintergreen Drive
Purcellville, VA 20132
www.HubertAstro.com

Prepared for
Kennedy Space Center, Florida

August 2008

NASA STI Program ... in Profile

Since its founding, NASA has been dedicated to the advancement of aeronautics and space science. The NASA scientific and technical information (STI) program plays a key part in helping NASA maintain this important role.

The NASA STI program operates under the auspices of the Agency Chief Information Officer. It collects, organizes, provides for archiving, and disseminates NASA's STI. The NASA STI program provides access to the NASA Aeronautics and Space Database and its public interface, the NASA Technical Reports Server, thus providing one of the largest collections of aeronautical and space science STI in the world. Results are published in both non-NASA channels and by NASA in the NASA STI Report Series, which includes the following report types:

- TECHNICAL PUBLICATION. Reports of completed research or a major significant phase of research that present the results of NASA Programs and include extensive data or theoretical analysis. Includes compilations of significant scientific and technical data and information deemed to be of continuing reference value. NASA counterpart of peer-reviewed formal professional papers but has less stringent limitations on manuscript length and extent of graphic presentations.

- TECHNICAL MEMORANDUM. Scientific and technical findings that are preliminary or of specialized interest, e.g., quick release reports, working papers, and bibliographies that contain minimal annotation. Does not contain extensive analysis.

- CONTRACTOR REPORT. Scientific and technical findings by NASA-sponsored contractors and grantees.

- CONFERENCE PUBLICATION. Collected papers from scientific and technical conferences, symposia, seminars, or other meetings sponsored or co-sponsored by NASA.

- SPECIAL PUBLICATION. Scientific, technical, or historical information from NASA programs, projects, and missions, often concerned with subjects having substantial public interest.

- TECHNICAL TRANSLATION. English-language translations of foreign scientific and technical material pertinent to NASA's mission.

Specialized services also include organizing and publishing research results, distributing specialized research announcements and feeds, providing information desk and personal search support, and enabling data exchange services.

For more information about the NASA STI program, see the following:

- Access the NASA STI program home page at http://www.sti.nasa.gov

- E-mail your question to help@sti.nasa.gov

- Fax your question to the NASA STI Information Desk at 443-757-5803

- Phone the NASA STI Information Desk at 443-757-5802

- Write to:
  STI Information Desk
  NASA Center for AeroSpace Information
  7115 Standard Drive
  Hanover, MD 21076-1320

NASA/TP—2013–217917

Behavior of Spinning Space Vehicles with Onboard Liquids, 2nd Edition, Technical Report B8030

Prepared by: Carl Hubert
Hubert Astronautics
644 Wintergreen Drive
Purcellville, VA 20132
www.HubertAstro.com

Prepared for:
Kennedy Space Center, Florida

National Aeronautics and
Space Administration

Kennedy Space Center
Kennedy Space Center, FL 32899-0001

August 2008

Available from:

NASA Center for AeroSpace Information
7115 Standard Drive
Hanover, MD 21076-1320
443-757-5802

Technical Report B8030
Contract Number NNK05LA48P

Behavior of Spinning Space Vehicles with Onboard Liquids

Second Edition

Prepared for
NASA/Kennedy Space Center

Prepared by
Carl Hubert
August 2008

NO RESTRICTIONS ON DISTRIBUTION

—

This document has been edited to remove sections that are subject to ITAR restrictions on distribution.

Hubert Astronautics, Inc.
644 Wintergreen Drive
Purcellville, VA 20132

www.HubertAstro.com

Contents

1. Introduction

1.1 Overview

Although the fundamental principles of spin stabilization are well established, uncertainty regarding the potential for rapid nutation growth caused by onboard liquids is a continuing concern. NASA and other organizations regularly encounter the issue of rapid nutation growth due to energy dissipation by liquids on spinning vehicles. Of concern is the stability of spinning upper stages and of spacecraft that spin for part or all of their missions. Several missions have required last-minute hardware or operational changes to deal with rapid nutation divergences that were identified late in the program. In some instances, major schedule slips were barely averted. In at least two cases, it was determined that a spinning upper stage was not a viable option.

Historically, the "slosh" issue has been addressed by each space vehicle project individually, if it has been addressed at all. Due to budgetary and programmatic constraints, individual projects are unable to address the problem globally. Hence, there has been little effort to collect available test and flight data and use that data to make a coherent, unified picture of the "slosh" effect and how to deal with it. To some extent, each project has had to "reinvent the wheel", which can be both costly and risky. This study is a step toward correcting the situation. Specifically, the goal was to identify and collect available flight and test data for spinning vehicles with onboard liquid propellants. A total of 149 flight data points and 1,692 test points were collected as part of this study. This data was analyzed, correlated, and is presented here in a normalized form. In most cases, the normalization involves a dimensionless nutation time constant that can be used to predict performance of other vehicles with the same type of tank. For some configurations, it was also possible to identify conditions that can lead to resonance between nutational motion and liquid modes. Gaps in the knowledge base are identified and approaches to filling those gaps are outlined.

The data presented here has two different but related uses. First, it can be applied directly to current and future spacecraft programs. Second, it can provide truth models for testing analytical techniques. Experience has shown that purely analytical models of the liquid "slosh" effect on spinning vehicles are unreliable unless they are validated against flight or test data. To the author's knowledge, this report contains the most extensive and varied data set available. As such, it should be a good resource for anyone seeking to develop and validate improved analytical techniques. All of the original digital data sets have been archived on disk, with copies provided to NASA/KSC. With some restrictions, many of these data sets can be made available to researchers within the United States.

Whenever possible, spacecraft are identified by name in this report. However, several organizations provided access to data with the explicit proviso that their programs not be identified and that parameters be presented only in normalized form. These constraints have been respected.

1.2 New in This Edition

In addition to numerous edits and clarifications, significant new material has been added to the following sections (some of which have been re-numbered):

Characteristics of Liquid Motion in Propellant Tanks:

3.4 Expanded to add a discussion of dynamic stability

Applying Flight and Test Data to Other Configurations:

5.1.7 New section on sensitivity to tank volume and the effect of using multiple small tanks instead of a single larger tank

5.1.9 New section on calculating dimensionless time constants from forced-motion test data

Spherical Tanks:

6.1.3 New section on off-axis tanks with "sponge" type propellant management devices

6.1.4 Expanded to add test results for a tank with very slender vanes

Spheroidal Tanks:

8.2 New section covering test and flight results for a nearly spheroidal tank (Dawn)

Cylinders and Tanks with Cylindrical Sections:

9.2 Expanded to add flight data (Deep Space 1)

9.3.2 Expanded to add flight data (Stardust)

9.4.1 Expanded to add flight data (Mars Global Surveyor)

9.4.4 Expanded to include additional test data plus flight data (Messenger)

9.5.2 Expanded to add flight data (Mars Climate Orbiter)

9.5.3 Expanded to add flight data (Mars Odyssey)

9.5.4 New section covering off-axis tanks

9.5.5 Expanded to include additional test data plus flight data (Messenger)

9.6 Expanded to add flight results for highly elongated tanks

9.7 Reorganized, added a discussion of longitudinal slosh modes, and added a plot of all modes that have been identified by secondary frequencies.

Tanks with Diaphragms or Bladders:

10.2.1 Expanded to add flight data (Deep Space 1)

10.2.2 New section covering flight results for off-axis spherical tanks with diaphragm attachment planes perpendicular to the spin axis (Genesis, Mars Pathfinder, and Mars Exploration Rover)

10.2.3 New section covering flight results for off-axis spherical tanks with diaphragm attachment planes parallel to the spin axis (Mars ’98 Lander and NEAR)

10.3.1 New section with test and flight data for a nearly spherical on-axis tank (Dawn)

10.4 Expanded to include additional drop test data, forced motion test data, and flight data for an on-axis tank with an aspect ratio of 1.11 (Deep Impact and New Horizons)

Summary of Propellant Tank Influences:

14.3 New section with general observations about using baffles

Index of NASA Missions Covered in This Report

17 New section that identifies which report sections cover NASA missions

2. Nutation and the Effect of Energy Dissipation

This section begins with a brief overview of rotational dynamics and defines terminology that is used throughout the report. This is followed by discussions of nutation sensing and the effect that kinetic energy dissipation has on nutation behavior.

2.1 Rigid-Body Rotational Dynamics

2.1.1 Rotational Equations of Motion

If we define **T** as the torque vector and **H** as the vehicle's angular momentum vector then the fundamental equation of rotational motion for a rigid body is

$$\mathbf{T} = \frac{d\mathbf{H}}{dt} \tag{2-1}$$

This equation is the rotational equivalent of Newton's second law and assumes that the differentiation is performed with respect to an inertially fixed reference frame. Although Equation 2-1 appears simple, it is an inconvenient form for analysis. It is far more useful to perform the differentiation with respect to a coordinate frame that is fixed in and rotates with the vehicle. If this is done, Equation 2-1 becomes

$$\mathbf{T} = \dot{\mathbf{H}} + \omega \times \mathbf{H} \tag{2-2}$$

where the dot over **H** denotes the time rate of change relative to a reference frame that is fixed in and rotates with the vehicle. If **I** is used to denote the vehicle's 3×3 inertia matrix and $\boldsymbol{\omega}$ denotes the angular velocity vector then we have

$$\mathbf{H} = \mathbf{I}\omega \tag{2-3}$$

$$\mathbf{T} = \mathbf{I}\dot{\omega} + \omega \times \mathbf{I}\omega \tag{2-4}$$

Note that Equation 2-4 assumes that **I** is constant. This is a good approximation if the liquid propellant represents a small fraction of the vehicle's total mass. For vehicles with relatively high liquid mass fractions Equation 2-4 and any analyses based upon it should be considered somewhat inaccurate. Despite this limitation, Equation 2-4 is a reasonable description of nutational motion and thus provides a foundation for evaluating flight and test performance with onboard liquids.

We now define an XYZ coordinate frame that is fixed in and rotates with the vehicle. For simplicity, X, Y, and Z are assumed to be principal axes. In other words, it is assumed that the off-diagonal terms in the inertia matrix are all zero. Although there is no loss in generality from making this assumption, it does mean that the X, Y, and Z-axes may have angular offsets from

the coordinate axes used for the vehicle's mechanical layout. Expanding Equation 2-4 into its three components yields *Euler's equations of motion:*

$$\begin{aligned} T_X &= I_{XX}\dot{\omega}_X + (I_{ZZ} - I_{YY})\omega_Y\omega_Z \\ T_Y &= I_{YY}\dot{\omega}_Y + (I_{XX} - I_{ZZ})\omega_X\omega_Z \\ T_Z &= I_{ZZ}\dot{\omega}_Z + (I_{YY} - I_{XX})\omega_X\omega_Y \end{aligned} \qquad 2\text{-}5$$

These relatively simple equations are widely used to analyze rotational motion. If the vehicle has no externally applied torques, the equations of motion reduce to

$$\begin{aligned} I_{XX}\dot{\omega}_X + (I_{ZZ} - I_{YY})\omega_Y\omega_Z &= 0 \\ I_{YY}\dot{\omega}_Y + (I_{XX} - I_{ZZ})\omega_X\omega_Z &= 0 \\ I_{ZZ}\dot{\omega}_Z + (I_{YY} - I_{XX})\omega_X\omega_Y &= 0 \end{aligned} \qquad 2\text{-}6$$

These coupled, nonlinear differential equations do not lend themselves to a general solution with a simple mathematical form. However, three simple steady-state solutions correspond to spin about each of the principal axes. For spin with a constant rate Ω about the Z-axis the steady-state solution is

$$\begin{aligned} \omega_X &= 0 \\ \omega_Y &= 0 \\ \omega_Z &= \Omega \end{aligned} \qquad 2\text{-}7$$

For a vehicle that is designed to spin, this is the intended nominal condition. In reality, however, perturbations from the nominal state will invariably occur. The next step, therefore, is to consider the effect of a small perturbation from the third solution:

$$\begin{aligned} |\omega_X| &<< \Omega \\ |\omega_Y| &<< \Omega \\ \omega_Z &= \Omega \end{aligned} \qquad 2\text{-}8$$

If the perturbation involves very small values for ω_X and ω_Y, we can linearize Equation 2-6 by making the approximation $\omega_X\omega_Y \approx 0$. This reduces the torque-free Euler equations to

$$\begin{aligned} I_{XX}\dot{\omega}_X + (I_{ZZ} - I_{YY})\Omega\omega_Y &= 0 \\ I_{YY}\dot{\omega}_Y + (I_{XX} - I_{ZZ})\Omega\omega_X &= 0 \\ I_{ZZ}\dot{\omega}_Z &= 0 \end{aligned} \qquad 2\text{-}9$$

These linearized equations of motion have a solution of the following form:

$$\begin{aligned} \omega_X &= A\cos(\lambda t) \\ \omega_Y &= B\sin(\lambda t) \\ \omega_Z &= \Omega \quad \text{(a constant)} \end{aligned} \tag{2-10}$$

Here, A and B are constants and λ is the *nutation frequency,* which is defined by

$$\lambda = \Omega\sqrt{\frac{(I_{ZZ} - I_{XX})(I_{ZZ} - I_{YY})}{I_{XX}I_{YY}}} \tag{2-11}$$

A and B are related to each other as follows

$$B = \pm A\sqrt{\frac{I_{XX}(I_{ZZ} - I_{XX})}{I_{YY}(I_{ZZ} - I_{YY})}} \tag{2-12}$$

In Equation 2-12, the positive sign is used if the vehicle is a *major axis spinner* (i.e., $I_{ZZ} > I_{XX}$ and $I_{ZZ} > I_{YY}$) and the negative sign is used if it is a *minor axis spinner* (i.e., $I_{ZZ} < I_{XX}$ and $I_{ZZ} < I_{YY}$). The cyclic solution given in Equation 2-10 is only valid if the nutation frequency has a real value. Validity thus requires that the vehicle be a major or minor axis spinner. If it is an *intermediate axis spinner* (i.e., $I_{XX} > I_{ZZ} > I_{YY}$ or $I_{YY} > I_{ZZ} > I_{XX}$), λ is imaginary and the solution is invalid.

2.1.2 Inertia Ratios and Inertial Symmetry

A dimensionless inertia ratio is a convenient indicator of a vehicle's rotational characteristics. Although space vehicles are often referred to as having a single inertia ratio, there are several different definitions of inertia ratio and it is important to know which one is relevant to a particular situation. For an inertially asymmetric vehicle ($I_{XX} \neq I_{YY}$), we can define the following fundamental inertia ratios

$$\begin{aligned} \sigma_X &= \frac{I_{ZZ}}{I_{XX}} \\ \sigma_Y &= \frac{I_{ZZ}}{I_{YY}} \end{aligned} \tag{2-13}$$

For a major-axis spinner these ratios are both greater than 1, for a minor-axis spinner they are both less than 1, and for an intermediate-axis spinner one ratio is greater than 1 and the other is less than 1. Applying the definitions in Equation 2-13 to Equation 2-11 yields

$$\lambda = \Omega\sqrt{(\sigma_X - 1)(\sigma_Y - 1)} \tag{2-14}$$

This clearly shows the relationship between the inertia ratios and the nutation frequency. If the vehicle is *inertially symmetric* ($I_{XX} = I_{YY}$), we can replace the two inertia ratios with a single inertia ratio, σ.

$$\sigma = \sigma_X = \sigma_Y \tag{2-15}$$

For an inertially symmetric vehicle we thus have

$$\lambda = \Omega\left|\sigma - 1\right| \qquad 2\text{-}16$$

For an *inertially asymmetric* vehicle ($I_{XX} \neq I_{YY}$), the relationship between the mass properties and the nutation frequency can be characterized by a single *effective inertia ratio.* This parameter is the inertia ratio of an equivalent inertially symmetric vehicle with the same nutation frequency as the asymmetric vehicle. From this definition of the *effective inertia ratio* we have

$$\sigma_{eff} = 1 \pm \sqrt{(\sigma_X - 1)(\sigma_Y - 1)} \qquad 2\text{-}17$$

$$\lambda = \Omega\left|\sigma_{eff} - 1\right| \qquad 2\text{-}18$$

In Equation 2-17, the positive sign is used for major-axis spinners and the negative sign is used for minor-axis spinners. Unless otherwise indicated, references in this document to "the inertia ratio" will indicate the effective inertia ratio. Physical constraints limit the effective inertia ratio to the following range:

$$0 < \sigma_{eff} < 2 \qquad 2\text{-}19$$

An effective inertia ratio of zero corresponds to an infinitely thin rod and a ratio of 2 corresponds to an infinitely thin disk. At these extremes, the nutation frequency equals the vehicle's spin rate. For physically realizable vehicles, the nutation frequency will always be less than the spin rate. It should also be noted that the nutation frequency is symmetrical about the inertia ratio of 1.0. For example, vehicles with inertia ratios of 0.8 and 1.2 have identical nutation frequencies if they are spun at the same rate. This means that any onboard liquids will be driven at the same frequency in the two configurations and will thus have similar energy dissipation characteristics. This symmetry means that test or flight data from a minor-axis spinner can be used to predict the behavior of a major-axis spinner and vice versa. A method for doing this is described in Section 5.

2.1.3 Importance of the Effective Inertia Ratio

Liquids in tanks on a spinning vehicle tend to have resonant modes with frequencies that are proportional to the spin rate. As Equation 2-18 shows, the nutation frequency is also proportional to the spin rate. If a liquid modal frequency and the nutation frequency are identical then a resonance will exist and rapid nutation growth can result. It is impossible to escape from this type of resonance by changing the spin rate because the liquid modal frequency and the nutation frequency are both proportional to the spin rate. Near a resonance, the vehicle's nutation characteristics can be very sensitive to small changes in the effective inertia ratio. This makes the effective inertia ratio a key parameter for evaluating the nutation performance of vehicles with onboard liquids.

2.1.4 Apparent Inertia Ratio

In this report, a distinction will be made between the *effective inertia ratio* and the *apparent inertia ratio.* As indicated in Section 2.1.1, the nutation characteristics discussed above are for a simple rigid body. The presence of onboard liquids alters the behavior and can shift the nutation frequency. To recognize this, we will define *effective inertia ratio* as applying to a vehicle with the liquid frozen in place and *apparent inertia ratio* as being that of an equivalent rigid body with the same nutation frequency as the vehicle with mobile liquid. The effective and apparent inertia ratios are usually close enough to each other that a distinction is not made between the two. However, if the vehicle's combination of mass properties and liquid characteristics place the system close to a resonance, or if the liquid represents a significant fraction of the vehicle's total mass or moments of inertia, it's possible for the effective and apparent inertia ratios to differ by as much as 20%.

2.1.5 Nutation Angle Defined

The degree of deviation from a state of simple spin about a principal axis is quantified by a parameter called the *nutation angle.* As shown in Figure 2-1, the nutation angle is the instantaneous offset between the angular momentum vector and the *principal axis* that the vehicle nominally spins about. Due to dynamic imbalances, the principal axis usually deviates slightly from the vehicle's intended spin axis. The nutation angle should be measured relative to the intended spin axis only if the intended spin axis is a principal axis. If the intended spin axis is not a principal axis, then the nutation angle should be measured relative to the principal axis that is nearest the intended spin axis.

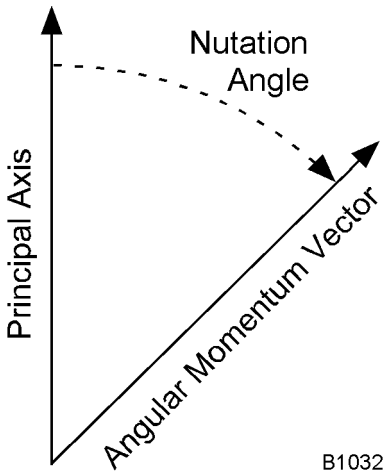

Fig. 2-1 Nutation Angle

If the vehicle is asymmetric ($I_{XX} \neq I_{YY}$), the nutation angle will vary at twice the nutation frequency. In this case, references to the nutation angle typically apply to the peak value during the course of the nutation cycle.

2.2 Sensing Nutation

As indicated by the mathematical treatment in Section 2.1.1, nutation leads to cyclic body rates about the transverse axes (the X and Y axes in the formulation used above). This suggests that the most direct way to sense nutation is with a gyro that is oriented to measure one of the transverse body rates. Although this is an excellent approach, an accelerometer can often provide equally good data at a lower cost. However, using an accelerometer as a nutation sensor requires some knowledge of how nutation affects linear acceleration at the unit's seismic center.

The cyclic angular rates and angular accelerations associated with nutation cause components to experience time-varying linear accelerations. If the vehicle is perfectly rigid (i.e., none of its components move relative to the 's nominal center of mass), the linear acceleration at a selected point in the vehicle body is given by

$$\mathbf{a} = \dot{\omega} \times \rho + \omega \times (\omega \times \rho) \qquad 2\text{-}20$$

where ω is the angular velocity vector and ρ is the vector from the vehicle's center of mass to the accelerometer's seismic center (Fig. 2-2). Most accelerometers are single-axis units. If **u** is a unit vector in the accelerometer's sense direction then the accelerometer output, a_{OUT}, is

$$a_{OUT} = \mathbf{u} \bullet \mathbf{a} \qquad 2\text{-}21$$

Figure 2-3 shows optimal accelerometer locations and orientations for sensing nutation. These locations and orientations are preferred because they avoid certain small nonlinearities and the biases associated with centripetal acceleration. For the two accelerometers shown in the figure, Equation 2-21 becomes

$$a_1 = (\omega_Y \Omega - \dot{\omega}_X)\rho_Z \qquad 2\text{-}22$$

$$a_2 = -(\omega_Y \Omega + \dot{\omega}_X)\rho_Y \qquad 2\text{-}23$$

Note that in these equations, ω_X and ω_Y are sinusoidal and essentially 90 degrees out of phase.

Although gyros and accelerometers are the best ways to measure nutation amplitude, frequency, and phasing, other sensors can provide limited nutation data. Of these alternatives, spinning sun sensors are probably the most common. The principal problem with using a sun sensor is that it provides only one data point per spin cycle, which is a relatively slow sampling rate when one is interested in a phenomenon that varies at nutation frequency. As the Lunar Prospector flight data in Figure 5-3 (Sec. 5.1.8) suggests, sun sensor output cannot easily be used to determine nutation frequency or phasing. However, with a sufficient number of data samples it is possible to get a reasonably good measurement of the rate of nutation growth or decay.

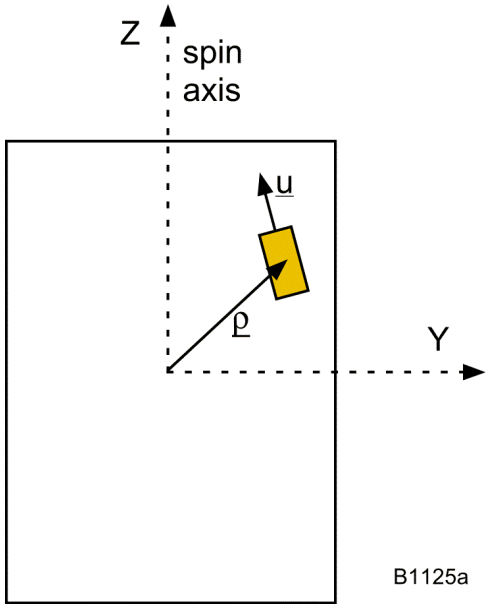

Figure 2-2 Accelerometer Sensing Geometry

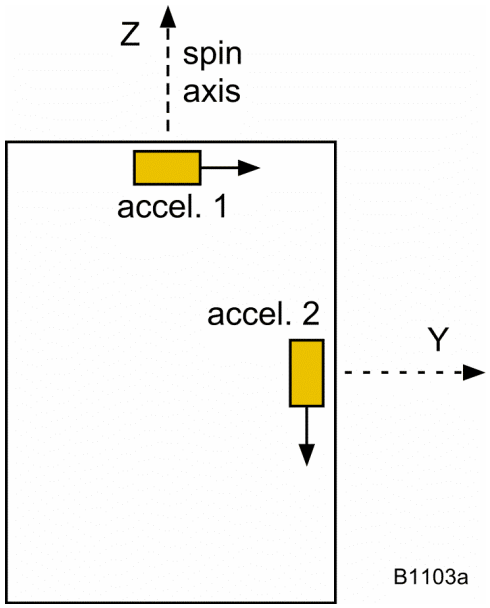

Figure 2-3 Ideal Sensing Geometries

2.3 Effects of Energy Dissipation

The cyclic accelerations associated with nutational motion cause onboard liquid propellants to flow within tanks. Viscosity effects associated with this flow cause some of the vehicle's rotational kinetic energy to be converted to molecular kinetic energy, which is also known as heat. Because the forces and torques associated with these viscosity effects are internal to the vehicle, there is no net effect on angular momentum; only the rotational kinetic energy changes. Depending on the vehicle's mass properties, this energy drain causes the nutation angle to either grow or decay. The characteristics of this behavior can be seen by examining the equilibrium kinetic energy. For simple spin about a principal axis, we have the following expressions for kinetic energy and angular momentum:

$$E = \frac{1}{2} I_{ZZ} \Omega^2 \qquad 2\text{-}24$$

$$H = I_{ZZ} \Omega \qquad 2\text{-}25$$

Equations 2-24 and 2-25 can be combined to yield

$$E = \frac{1}{2} \frac{H^2}{I_{ZZ}} \qquad 2\text{-}26$$

Equation 2-26 shows that for a given angular momentum, spin about the minor axis is an energy maximum and spin about the major axis is an energy minimum. As previously noted, internal energy dissipation mechanisms have no effect on the vehicle's angular momentum. This means that energy dissipation will cause the vehicle to ultimately converge to a state of simple spin about the major axis. In other words, nutation about the major will be damped by the motion of onboard liquids. Conversely, a small perturbation from a state of simple spin about the minor axis will grow unless restrained by an active nutation control system. The case of minor-axis spin is particularly important because stacking a spacecraft on a spinning upper stage invariably creates a configuration that spins about its minor axis. Quantifying the effects of energy dissipation on these configurations is the motive for the present study.

2.3.1 Linear Energy Dissipation

Passive energy dissipation causes the nutation amplitude to change exponentially if the dominant dissipation mechanism is viscous damping. Viscous damping is also known as linear damping because the associated forces and torques are proportional to the relative rate between two components (e.g., between a liquid propellant and the tank wall). On a nutating vehicle with linear damping, the mean energy dissipation rate is proportional to the square of the amplitude of the transverse angular rate (the cyclic angular rate perpendicular to the nominal spin axis). This, in turn, means that the energy dissipation rate is proportional to the nutation angle squared. Exponential nutation growth or decay is described mathematically by the following equation.

$$\theta = \theta_0 e^{t/\tau} \qquad 2\text{-}27$$

Here, θ_0 is the initial nutation angle, t is time, and τ is the nutation time constant. The last parameter is the time required for the amplitude to change by a factor of 2.718. Nutation growth is characterized by a positive time constant and decay by a negative time constant.

2.3.2 Nonlinear Energy Dissipation

As the discussion in the previous subsection suggests, exponential nutation change occurs only if the energy dissipation mechanism is linear. With other dissipation mechanisms or growth characteristics, it is improper to characterize the nutation behavior as having a "time constant". A good example of nonlinear behavior is the "nutation synchronous" mode described in Section 3.1 and discussed further in Section 5.2.2. This type of behavior, which occurs only in centerline tanks, is characterized by a unidirectional swirling flow. This flow is at an essentially constant rate that is independent of nutation amplitude, for amplitudes up to about 10 degrees. The energy dissipation rate due to this type of liquid motion is thus independent of nutation amplitude. In other words, kinetic energy loss is more like that due to Coulomb friction than viscous friction. As discussed in Section 5.2.2, Culomb friction causes nutation to grow as the square root of time.

3. Characteristics of Liquid Motion in Propellant Tanks

Although motion within propellant tanks is often referred to by the generic term "sloshing", there are actually three completely different types of liquid behavior that affect nutation dynamics and rotational stability: bulk motion, surface wave sloshing, and subsurface inertial waves. These behaviors are illustrated in Figure 3-1.

3.1 Free Surface Sloshing

As shown in Figure 3-1, sloshing is an undulation of the free surface. As such, it can only occur in partially filled tanks. Small-amplitude sloshing typically involves a cyclic surface oscillation at a well-defined frequency. Except when the tank has a low fill fraction, small-amplitude sloshing causes relatively little liquid movement at the bottom of the tank. Large-amplitude sloshing is more complex, and can involve splashing and breaking waves. This more violent behavior usually occurs in response to sharp transients, such as solid motor ignition and burnout.

In most tanks that are offset from the vehicle's spin axis, the lowest sloshing frequency is well above the nutation frequency. This precludes a strong interaction between free-surface sloshing and nutational motion. Under such conditions, surface waves are usually small and have only a second-order effect on energy dissipation. However, if the spin axis passes through a tank, the dynamics are quite different and vigorous large-amplitude surface waves can occur. This behavior, which is shown conceptually in Figure 3-2, is variously known as a "swirling", "rotary slosh", or "nutation synchronous" mode. As the figure shows, the motion is characterized by a wave that swirls around the tank at the nutation frequency. The further a partially-filled centerline tank is from the vehicle's center of mass, the easier it is to excite this behavior and the more vigorous the motion will be once it starts. On a minor-axis spinner the wave is retrograde. In other words, when viewed from a coordinate frame fixed on the vehicle, the wave moves around the tank in a direction opposite to the spin. On a major-axis spinner the wave is prograde, meaning that the flow is in the same direction as the vehicle's spin.

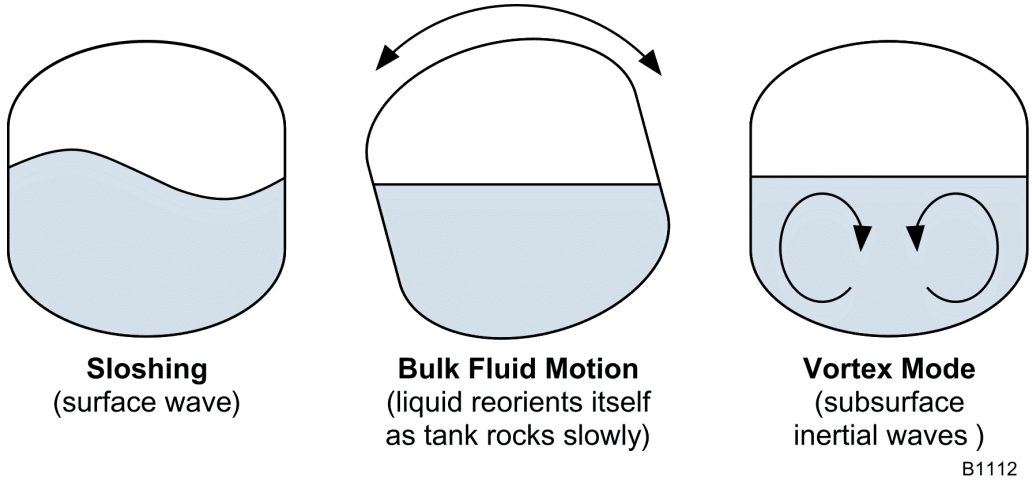

Figure 3-1. Three types of liquid motion

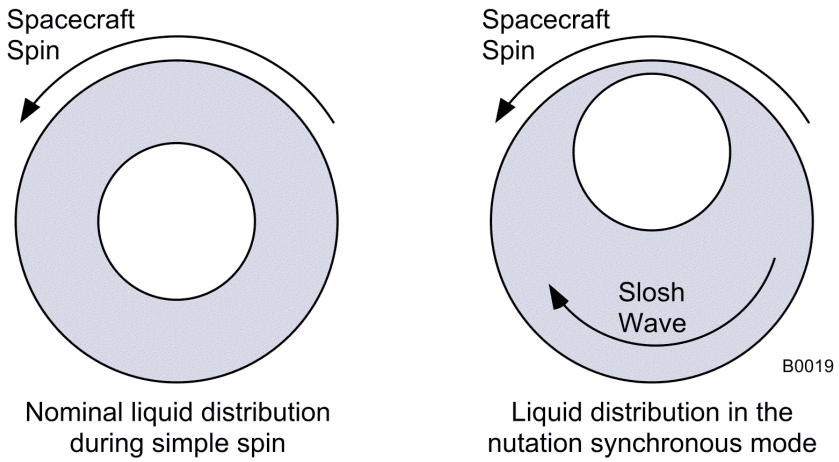

Figure 3-2. Liquid Behavior during Nutation Synchronous Motion on a Minor-Axis Spinner (view is down the vehicle spin axis)

Nutation synchronous motion typically has two phases. The first is a mode transition during which liquid pools toward one side of the tank and – after a period of increasingly large oscillations – begins swirling around the tank at the nutation frequency. This transition can be extremely rapid, with the mode being completely established within 2 or 3 nutation cycles. The immediate effect of this mode transition is that it establishes a rotating dynamic imbalance, which is visible as an extremely rapid jump in the nutation amplitude. Harrison (1987) refers to this type of behavior as a "momentum transfer mode" because it involves an exchange of angular momentum between the liquid and the rest of the vehicle with no significant change in kinetic energy. Once the nutation synchronous mode is established, unidirectional flow rapidly dissipates kinetic energy. Although nutation amplitude does not change as rapidly during this second phase as it does during the mode transition, it can still be quite rapid. This can be a serious problem if the vehicle is a minor-axis spinner.

Nutation synchronous motion in on-axis tanks is a complex phenomenon that has seen little mention in the published literature. There has, however, been substantial mathematical and experimental treatment of a similar behavior in circular heat pipes and viscous ring nutation dampers. The problem was discussed by O'Hern et al. (1972), who analyzed the 1969 ATS-V mission failure that dramatically demonstrated how small quantities of liquid can severely affect the stability of a spinning vehicle. ATS-V experienced an uncontrollable 11-second divergent nutation time constant after upper stage burnout. This caused the vehicle to enter flat spin and the mission was lost. The loss was ultimately attributed to energy dissipation by liquid ammonia in sixteen circumferential heat pipes.* Of the vehicle's 452 kg, only 1.2 kg was liquid. Nutation synchronous flow in partially filled viscous-ring nutation dampers has been addressed by Cartwright et al. (1963), Alfriend (1974), Mingori and Harrison (1974), Hubert (2000), Hubert and Swanson (2001), and others.

* The ATS-V heat pipes were circular hoops that were centered on and perpendicular to the vehicle's spin axis.

3.2 Bulk Fluid Motion

Bulk fluid motion is characterized by liquid reorienting itself within a tank in response to changes in the tank's alignment relative to the acceleration field and/or inertial space. For example, when a half-filled coffee cup is slowly tilted, the free surface remains horizontal as the liquid repositions itself to minimize its gravitational potential energy. If the cup is slowly rocked back and fourth, the liquid continually reorients itself relative to the sides of the cup with little or no rippling of the free surface. This behavior is shown in the middle illustration in Fig. 3-1.

On a spinning vehicle bulk fluid motion is similar to that of the coffee cup example except that the liquid is held in place by centrifugal force instead of gravity and the free surface is a cylindrical segment instead of flat. Nutation produces a cyclic bulk motion that dissipates energy due to viscous drag as the liquid flows past the tank walls and propellant management devices.* Unlike free-surface sloshing, bulk motion affects the entire body of the liquid. This means that it can produce much more flow past a PMD than simple surface wave motion. This, in turn, means that under non-resonant conditions bulk motion can dissipate far more energy than free-surface sloshing. On vehicles with off-axis spherical tanks, bulk motion past PMD's is usually the principal energy dissipation mechanism.

It is worth noting that, unlike sloshing, bulk motion can exist without a free surface. In other words, it can occur in a 100% full tank. Cyclic rotation during nutation causes the tank walls and PMD to move relative to the contained liquid even if the tank has no ullage volume. For some tank configurations, energy dissipation is greatest when the tank is 100% full.

Bulk fluid motion can also occur in diaphragm tanks. Even if the diaphragm is stiff enough to hold its shape during small-amplitude nutation, the cyclic rotations associated with nutation will cause bulk fluid motion relative to the tank walls and relative to the diaphragm. Because diaphragms typically cause the fluid-filled cavity to be non-spherical, the liquid motion is potentially more vigorous and thus potentially dissipates more energy than would be dissipated by a completely filled spherical cavity.

3.3 Inertial Waves (Vortex Modes)

Inertial waves involve subsurface circulation with very little free surface motion. Because the free surface is not directly involved, these waves can exist in a 100% full tank. Inertial waves are driven by cyclic pressure waves from nutation-induced angular motions of the tank wall coupled with Coriolis forces. The involvement of the Coriolis effect means that these inertial waves cannot be replicated in non-spinning tank tests. It also means that analytical modeling of inertial waves is much more difficult than the modeling of liquid motion on a non-rotating vehicle. In particular, the nature of the motion is such that it cannot be emulated by the equivalent pendulum models that are often used to assess liquid/vehicle interactions. This

* In reality, the primary movement is of the tank relative to the fluid. This is especially true for a spherical tank.

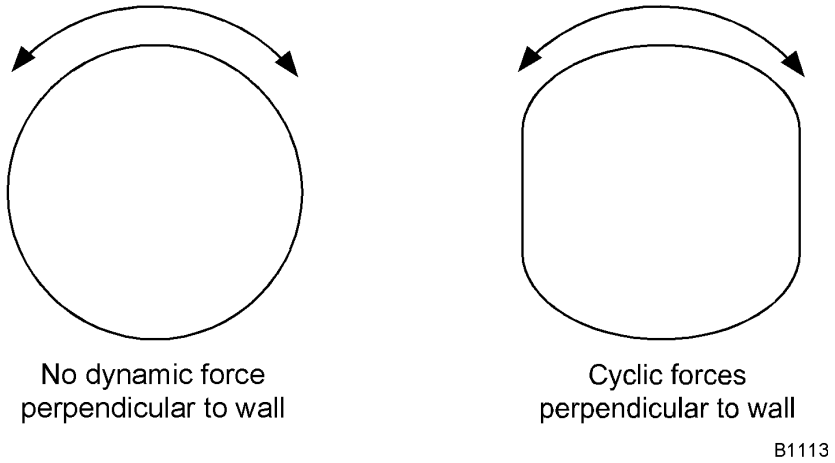

Figure 3-3. Cyclic rotation produces force components perpendicular to the tank wall in non-spherical tanks, but not in spherical tanks

limitation on pendulum models is serious because inertial waves are often the principal energy dissipation mechanism in non-spherical tanks.

Like surface waves, inertial waves have distinct natural frequencies that are a function of tank shape and fill level. However, unlike surface waves in off-axis tanks, inertial waves can have natural frequencies that are well below the spin rate. This means that inertial waves can resonate with nutational motion to produce rapid energy dissipation. These resonances are often very sharp, which means that near a resonance relatively small changes in vehicle inertia ratio or tank fill fraction can produce dramatic changes in nutation growth rates.

Although inertial wave modes can theoretically exist in tanks of any shape, they can only be excited in non-spherical tanks. As shown in Figure 3-3, cyclic angular motion causes a spherical tank's wall to move in a direction parallel to the wall, and this motion couples with the contained liquid only weakly through viscous shear forces. With a non-spherical tank, however, cyclic angular motion gives the tank wall a component of linear displacement that is perpendicular to the wall. This perpendicular displacement can produce a vigorous motion within the contained liquid.

3.4 Dynamic Stability and Wobble Amplification

The term "spin stability" is often used interchangeably to describe two independent phenomena. The following definitions are therefore introduced to avoid confusion:

Equilibrium Spin Axis: The axis that a vehicle spins about when there is no nutation.

Spin-Axis Stability: The stability of the equilibrium spin axis within the vehicle's body. A stable equilibrium spin axis has a constant orientation in body coordinates. On some vehicles, unconstrained propellant shifts, especially flow through manifolds that connect tanks, can cause spin-axis instability.

Nutational Stability: The stability of nutational motion about the equilibrium spin axis—assuming no active nutation damping. If nutation damps passively, the vehicle is

nutationally stable. If nutation grows without active control, the vehicle is nutationally unstable.

On spinning vehicles, bulk motion affects spin-axis stability, independent of the rate of energy dissipation [Nayfeh and Meirovitch, 1974; McIntyre and Miyagi, 1976; McIntyre and McIntyre, 1982; Agrawal, 1982; Hubert et al. 1988; Pocha, 1995]. For a vehicle spinning about its maximum moment of inertia axis the issue is "wobble amplification." A dynamic imbalance tilts the equilibrium spin axis relative to its nominal orientation within the vehicle. This tilt causes mobile liquids to relocate consistent with the changed centripetal acceleration field. The liquid displacement in turn amplifies the dynamic imbalance and causes a further shift in the liquid. Depending on the tank configuration, the ultimate equilibrium spin axis can be offset from the intended spin axis by a fraction of a degree or by tens of degrees.

Wobble amplification is usually not a problem for vehicles that spin about their minor axes because an offset spin axis causes liquid displacements that partially correct the dynamic imbalance. If the tank has a diaphragm, however, the dynamic imbalance and resulting spin axis offset can be larger than would be expected with a non-diaphragm tank. In a partially filled diaphragm tank, the diaphragm assumes a wrinkled shape that can differ substantially from the nominal cylindrical liquid free surface in a non-diaphragm tank. Depending on the degree of asymmetry in the surface shape, this deviation from cylindrical can produce a significant dynamic imbalance and spin axis offset.

A full description of the wobble amplification phenomenon is beyond the scope of this report. Interested readers can find more information in the papers mentioned above.

4. Nutation Testing

4.1 The Need for Testing

Although progress has been made in the ability to analytically predict liquid resonant frequencies, analytical methods often grossly underestimate the effect that these resonances have on nutation growth rates. Analytical predictions of resonant nutation time constants are frequently in error by an order of magnitude or more. Furthermore, purely analytical methods for determining nutation time constants are notoriously unreliable even for non-resonant conditions. In recognition of this difficulty, some efforts have focused on trying to analytically determine worst-case lower bounds on divergent nutation time constants instead of trying to predict actual time constants within some level of uncertainty. Although these methods have achieved limited success, they are typically based on equivalent mechanical models that may not reflect the full range of possible liquid motions. History has shown that predictions of nutation growth rates are only reliable if the analytical model is based on flight or test data that applies directly to the configuration under consideration. Even validated models must be used with care because they can be inaccurate for nutation angles that exceed a few degrees. The nonlinear behavior associated with large-amplitude liquid motion can lead to different nutation growth characteristics than one might expect from a small-angle model.

Numerous tests and flight experiences have shown that liquids on spinning vehicles can have very sharp resonances, with small deviations from previously tested or flown configurations producing dramatically different nutation growth rates. This report includes many examples of such behavior. Thus, there is a need for caution when applying existing flight and test data to new configurations. This is especially true if a tank has a shape, orientation, or PMD that has never been used on a spinning vehicle. To assure success, a vehicle configuration must be within the parameter space of previously tested or flown configurations. This parameter space includes vehicle inertia ratio, tank shape, tank fill fraction, tank location relative to the vehicle center of mass, tank orientation, propellant management device shape and stiffness, etc. Attempts to predict nutation behavior by interpolation between closely spaced test and flight data points have generally been successful. However, extrapolation outside the range of available data has proven to be risky.

4.2 Test Considerations and Limitations

Of all considerations relating to nutation time constant testing, perhaps the most important is that the test platform must spin. This is necessary because the Coriolis effect plays a prominent role in the fluid dynamics and because it is essential to accurately model the liquid's in-flight free surface. Accurate emulation of the free surface naturally occurs with free-fall test methods. However, to achieve this with other methods may require a very high spin rate, especially if the tank is to be mounted on or near the vehicle's spin axis. Figure 4-1 illustrates this issue for a

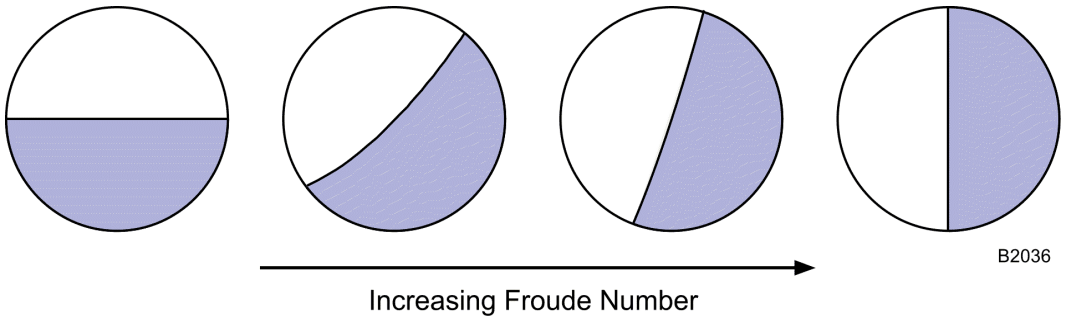

Figure 4-1. Free Surface in an Off-Axis Tank during Non Free-Fall Testing

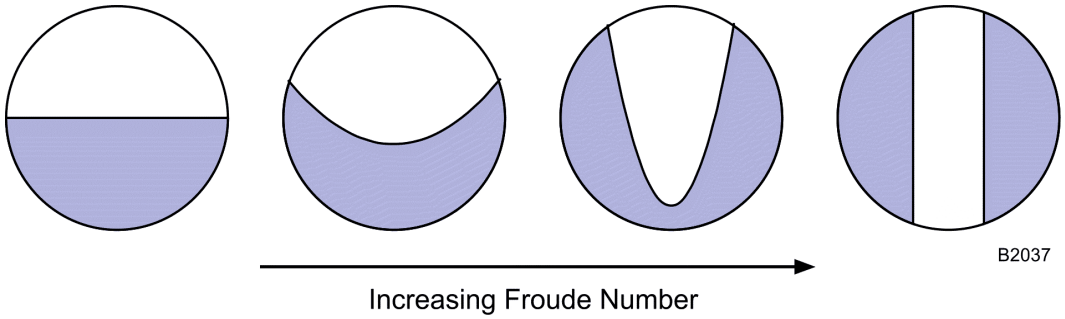

Figure 4-2. Free Surface in an On-Axis Tank during Non Free-Fall Testing

spherical tank that is offset from the spin axis. The tank on the left has a Froude number* of zero (no spin) and the contained liquid has a flat free surface. The tank on the right has a Froude number of infinity (zero g) and the liquid has a cylindrical free surface. The free surfaces of the middle two tanks are paraboloids. The faster the test platform spins, or the further the tank is from the spin axis, the easier it is to achieve a high Froude number and to thereby approximate the condition that exists in space. Figure 4-2 is similar to Figure 4-1 except that it shows a spherical tank that is mounted on the vehicle's spin axis.

The importance of achieving a high Froude number was clearly demonstrated during an extensive series of air bearing tests of EXOSAT's off-axis spherical propane tank [Marcè, et al. (1981)]. During one test series with a fill fraction of 0.70, increasing the Froude number from 2.05 to 3.61 resulted in a 50% reduction in the nutation time constant. Another test series yielded a 72% NTC reduction when the Froude number was increased from 2.33 to 8.15. In all cases, higher Froude numbers yielded shorter time constants. For EXOSAT, predictions of flight performance were made by running tests over a wide range of Froude numbers and analyzing the trends to determine the asymptote that corresponded to the flight Froude number of infinity.

Another issue that may need to be addressed by testing is the potential for coupling between the vehicle's rigid body dynamics and fluid dynamics. This coupling is inherently modeled by free fall techniques, but cannot be modeled during forced motion tests. Furthermore, depending on the nature of the dynamic interaction, it may not be modeled in air bearing tests.

* The ratio of centrifugal force to axial force. The Froude number is essentially infinite during simple spin in orbit but can be low when the vehicle is thrusting to change its orbit or during some types of ground-based testing.

This is an issue if the fluid's mass or moment of inertia is a large fraction of the vehicle's total mass or MOI, or if the configuration of interest involves a large tank with a low fill fraction (i.e., if the liquid center of mass can experience very large time-varying displacements).

4.3 Scale Models

All of the test methods described in the next section can be implemented with scale models. For free-fall techniques (drop and ballistic trajectory tests), subscale modeling is usually the only option. Scale modeling involves identifying key dimensionless parameters and designing a model that has the same values for these parameters as the actual vehicle. For nutation testing, dimensionless parameters are based on the following dimensioned parameters:

a.....inertial acceleration at the liquid's free surface
I_S.....spin axis moment of inertia
I_T.....transverse axis moment of inertia
L .....typical length, such as the distance from the vehicle cm to the tank center
m.....total vehicle mass
r .....distance from the spin axis to the liquid free surface
R .....tank radius
t .....time
ρ_L.....liquid density
ν .....liquid kinematic viscosity
Ω .....spin rate

For most vehicle operations of interest, the inertial acceleration is zero. The principal exception occurs when a rocket engine is being fired to change the vehicle's trajectory in space. During free-fall tests, a is essentially zero. During other types of testing a is usually equal to the acceleration of gravity.

A scale model will have the same nutation performance as the actual vehicle if the following dimensionless parameters are preserved in the scaling:

Length .....R/L
Mass .....$\rho_L R^3/m$
Moment of inertia .....$\rho_L R^5/I_S$
Inertia ratio.....I_S/I_T
Time .....Ωt
Reynolds number .....$R^2\Omega/\nu$
Froude number.....$r\Omega^2/a$

Some of these dimensionless parameters are more important than others. For example, it is essential that the model's inertia ratio match that of the actual vehicle. On the other hand, as will be discussed in Section 5.1, there is usually only a weak sensitivity to Reynolds number and thus that particular parameter need not be exact. Mass and moment of inertia scalings also need not

be exact if the liquid represents only a small fraction of the vehicle's total mass and moment of inertia. Note that mass and moment of inertia scaling is impossible when using forced-motion methods, and mass scaling is impossible in air-bearing tests. This makes those particular methods unsuitable if onboard liquid represents a sizeable fraction of the vehicle's total mass or moment of inertia.

For a non-thrusting vehicle in space, the Froude number is essentially infinite. This condition can easily be matched during free-fall testing but not by other test techniques. If a model cannot emulate an infinite Froude number, the value should be at least 10 for an off-axis tank and much higher than that for an on-axis tank. Even for an off-axis tank, a Froude number of 10 may be marginal for accurate time-constant determination. Some organizations consider Froude numbers less than 40 to be too low even for an off-axis tank.

The dimensionless time (Ωt) is of particular importance in free-fall testing because such tests by their nature must be limited to a few seconds in duration. This limitation is overcome by spinning the model at a much higher rate than the actual vehicle. For example, if the model is spun 50 times faster than the actual vehicle, each second of test time represents 50 sec in flight.

If the tank to be tested contains a diaphragm, bladder, or flexible propellant management device (PMD) two additional dimensionless parameters must be preserved in the scale model. To define these dimensionless parameters we must introduce three additional dimensioned parameters:

d.....PMD thickness
E.....Young's modulus
ρ_P.....PMD density

These parameters plus those defined earlier are used to compute the dimensionless parameters associated with PMD flexibility:

Static response to centrifugal force..... $\rho_P R^4 \Omega^2/(Ed^2)$
Dynamic response to liquid motion..... $\rho_L R^5 \Omega^2/(Ed^3)$

If the tank to be tested contains a diaphragm or bladder, this scaling can be difficult. For a subscale model, the principal challenge is finding a material that will both accurately scale the stiffness and survive the test environment. At first glance, full-scale forced-motion or air bearing tests with actual diaphragms or bladders may seem to avoid the materials issue. However, the spin speeds needed to achieve an adequate Froude number may be such that the static and dynamic scalings identified above cannot be preserved.

4.4 Test Methods

4.4.1 Drop Tests

The drop test method involves spinning-up and then dropping an instrumented scale model that has been developed according to the scaling laws described in Section 4.3. The test article must be subscale because even the tallest drop towers cannot give enough "zero-g" time to adequately

test a full scale model. The test spin rate is typically between 1000 and 3000 rpm. The model must thus be sufficiently robust that it will not fly apart during test or be damaged during the sudden deceleration at the end of a drop. For more about the drop test method see Harrison (1984, 1987), Harrison et al. (1983), Pocha (1987), and Guibert (1987).

4.4.2 Ballistic Trajectory Tests

Ballistic trajectory tests are similar to drop tests in that they both involve free-fall and that both typically involve subscale models. The principal difference is that drop tests are conducted in a tower and ballistic trajectory tests are conducted in an aircraft (e.g., NASA's "Vomit Comet"). An advantage to testing in an aircraft flying a ballistic trajectory is that test times can be much longer: up to 10 seconds on an aircraft, versus 1.25 seconds in a drop tower. This advantage however is largely negated by the fact that the spin rate must be limited to several hundred rpm for safety reasons. Furthermore, tests requiring an aircraft can be quite expensive. Reiter and Lee (1966) were the first to conduct tests of this type. To this writer's knowledge, their paper was also the first to describe subscale nutation testing.

4.4.3 Air-Bearing Tests

The air-bearing method involves constructing an inertially equivalent mock-up of the vehicle with correctly located propellant tanks and a spherical air bearing at the center of mass. The configuration can be either full scale or subscale. The test article is spun-up and a restraining hub is then retracted to allow full 3-axis rotational motion. Nutation is typically monitored using an accelerometer or gyro mounted on the rig, with data being telemetered to a recording device elsewhere in the test facility. Air bearing tests are often conducted in altitude chambers to avoid the distorting effects of aerodynamic drag.

Air bearing tests have been successfully conducted for numerous tank configurations, and because test runs can last an hour or more, it is the best approach for measuring long nutation time constants.* However, like all test methods, it does have limitations. First, as mentioned previously, it may be difficult to spin the rig fast enough to achieve a sufficiently high Froude number, especially if the tests are of a full-scale tank or if the tank is mounted on the spin axis. Second, rigs with very low inertia ratios can be difficult to build and operate unless the spin axis is horizontal instead of vertical, and horizontal rigs are impractical for nutation time constant testing because they must spin extremely rapidly to minimize the effect of cyclic gravitational forces on the liquid. Third, the method cannot model coupling between the vehicle's cm motion and the liquid's cm motion. This is an issue if the liquid mass is a large fraction of the vehicle's

* Earth's rotation is often the limiting factor on air bearing run duration. The spinning rig has a large angular momentum and with essentially no external torque, the rig's angular momentum vector maintains a constant orientation in inertial space. As Earth rotates under the platform, the rig appears to change its orientation relative to the chamber, although it is the chamber that is actually changing its orientation relative to the spinning rig. Since tests usually start with the spin-axis vertical, the magnitude of this effect is greatest for test sites at the equator and least for test sites at high latitudes. Air bearing rigs are typically limited to a 15 or 20-degree displacement before the test must be halted.

total mass. Finally, running tests in an altitude chamber means that time is required to pump out the air after each change of inertia ratio or fill fraction. This limits the number of configurations that can be tested in a day.

For more about air bearing tests see Peterson (1976), Marcè et al. (1981), Hubert and Goodzeit (1983), and Pawlowski and Imbert (1984).

4.4.4 Forced Motion Tests

Forced-motion testing involves mounting a tank on a motor-driven rig that spins and "nutates" in a manner that emulates the vehicle's motion in space. Unlike other test methods, which measure nutation change directly, the forced-motion method requires indirect measurement. One measurement approach is to use load cells on the tank mounts to determine forces and torques associated with liquid motion, and then using those to determine the effect that the liquid would have on a nutating vehicle. An alternative method is to measure the current required by the drive motors with and without the liquid. The difference can then be used to calculate the energy dissipated by the liquid for a given nutation amplitude, and this in turn can be used to determine a nutation time constant.

Among the advantages of the forced motion method is that, once the tank is mounted and filled, one can run numerous tests that emulate a wide range inertia ratios in a very short period of time. It is also possible to mount a video camera on the spinning platform to record the exact nature of the liquid motion, something that can be difficult to do with small free-fall models. The forced-motion method, however, has some of the same limitations as the air-bearing test method. Specifically, it does not model the vehicle's cm motion, which can be an issue if the liquid mass is a large fraction of the vehicle's total mass. It may also be difficult to spin the rig fast enough to achieve a sufficiently high Froude number, especially if the tests are of a full-scale tank or if the tank is mounted on the spin axis. Finally, because the measurements are indirect, the forced-motion method requires more extensive data processing and interpretation than the other methods described above.

Forced motion testing usually involves steady state motion at a constant nutation angle. This restriction means that the method cannot characterize transients or identify energy dissipation mechanisms that are nonlinear functions of nutation angle. Analysis of test data usually involves an implicit assumption that linear energy dissipation mechanisms predominate, but this assumption cannot be confirmed using the test data. Fortunately, because drop tests and flight performance indicate that most tank configurations involve linear behavior, linearity is usually a safe assumption for forced motion tests.

For more about forced motion testing see Vanyo and Likins (1971), Vanyo (1973), Zedd and Dodge (1985), Guibert (1986), Wilde (1997), Deffenbaugh et al. (1998), and Green and Burkey (2007).

4.4.5 Comparison of Test Methods

Table 4-1 compares the advantages and disadvantages of the four test methods. Most of the characteristics in the table have been mentioned above, but several are worth further discussion.

First, although unconstrained center of mass motion (i.e., coupling between liquid and rigid body dynamics) can only be modeled using free fall techniques, this is not an issue when the liquid represents a small fraction of the vehicle's total mass or moment of inertia. However, if the vehicle does have a large liquid mass fraction there are key behaviors that can only be detected with free-fall methods. Among these are mode shape and modal frequency shifts that are only detectable if the cm is free to move. In flight, the vehicle's true center of mass (and center of rotation) moves as the liquid moves. The liquid motion also shifts the nutation frequency to a value other than what it would be if the liquid were frozen in place. This frequency shift is difficult to determine analytically. These modeling problems can be an issue if the liquid (all tanks combined) represents 20 percent or more of the vehicle's total mass or moment of inertia.

Table 4-1. Test Method Comparison

Characteristic	**Fixed Center of Rotation**		**Free Fall**	
	Air Bearing	**Forced Motion**	**Ballistic (Aircraft)**	**Drop Test**
Measurement	nutational motion	load cell or motor current	nutational motion	nutational motion
Unconstrained center of mass?	no	no	**yes**	**yes**
Insensitive to 1-g effects?	no	no	**yes**	**yes**
Can measure long time constants?	**yes**	doubtful	no	no
Quick change of PMD or baffle?	no	no	no	**yes**
Can model low inertia ratio?	difficult	**yes**	**yes**	**yes**
Can model inertial asymmetry?	limited	no	**yes**	**yes**
Quick change of inertia ratio	no	**yes**	no	**yes**
Can test full-scale tanks	**yes**	**yes**	no	no
Can test a range of nutation angles	**yes**	no	**yes**	**yes**

The reference in Table 4-1 to "quick change of PMD or baffle" reflects an ability to react to tests that show unacceptable nutation time constants. If test results indicate that a configuration cannot meet nutation performance requirements it may be necessary to modify the propellant management device or add a baffle. To date, subscale drop testing is the only method that has demonstrated an ability to support rapid assessment of alternate designs, with as many as 3 or 4 different baffle designs tested in a single day.

5. Analyzing Flight and Test Data, and Applying the Results to Other Configurations

This report presents test and flight results in a normalized form that can be scaled to predict the nutation behavior of configurations that have not yet flown. The methods used to analyze and normalize the available data are described in this section.

5.1 Exponential Nutation Growth or Decay

Passive energy dissipation causes nutation amplitude to change exponentially if the dominant dissipation mechanism is viscous damping. Viscous damping is also known as linear damping because the associated forces and torques are proportional to the relative rate between two components (e.g., between a liquid propellant and the tank wall). On a nutating vehicle with linear damping the mean energy dissipation rate is proportional to the square of the amplitude of the transverse angular rate (the cyclic angular rate perpendicular to the nominal spin axis). This, in turn, means that the energy dissipation rate is proportional to the nutation angle squared. Exponential nutation growth or decay is described mathematically by the following equation.

$$\theta = \theta_0 e^{t/\tau} \qquad 5\text{-}1$$

Here, θ_0 is the initial nutation angle, t is time, and τ is the nutation time constant. The last parameter is the time required for the amplitude to change by a factor of 2.718. Nutation growth is characterized by a positive time constant and decay by a negative time constant.

5.1.1 Dimensionless Time Constants

Nutation time constants can readily be determined from flight or test data. However, to apply nutation data from one vehicle configuration to a different vehicle, it is necessary to apply scaling laws such as those described in Section 4.3. Examination of the system dynamics shows that the nutation time constant is a function of the following parameters:

N.....number of tanks

r .....tank radius (interior measurement)

d .....radial offset of the tank center (measured from the vehicle spin axis)

h .....axial offset of the tank center (measured from the vehicle cm)

FF .....liquid fill fraction (fraction of the tank volume occupied by liquid)

ρ .....liquid density

R_e.....Reynolds number

I_S.....vehicle spin-axis moment of inertia

σ_{eff}.....vehicle effective inertia ratio (see Section 2.1.2 for a definition)

Ω .....vehicle spin rate

Tests by McIntyre (1984), Marcè, et al. (1981), and others have shown that in most cases the nutation time constant is relatively insensitive to R_e. Nutation behavior has also been shown to be relatively insensitive to h and d when the spin axis does not pass through the tank, or when the fill fraction is close to 1.0.* On the other hand, flight and test performances have repeatedly shown strong nonlinear sensitivities to fill fraction, inertia ratio, tank shape, and the configuration of internal hardware such as diaphragms, baffles, and propellant management devices.

Based on observations from dimensional analysis, Neer and Salvatore (1972) introduced a time constant scaling concept, which they referred to as a "time constant group." Their method, which worked well, was subsequently used by Agrawal (1984), McIntyre (1984), and others. Because of its past success, a variant of the Neer-Salvatore scaling approach was used to calculate the *dimensionless time constants* (DTC's) that appear in subsequent sections of this report. The DTC (T_D) is defined by the following equation:

$$T_D = N\left(\frac{\rho r^5}{I_S}\right)\Omega\tau \qquad 5\text{-}2$$

Note that the term ρr^5 in Equation 5-2 is proportional to the self-inertia of the liquid within a tank.† Known values of T_D can be used to determine the time constant for another vehicle with the same type of tank by applying the inverse of Equation 5-2.

$$\tau = \left(\frac{I_S}{N\rho r^5\Omega}\right)T_D \qquad 5\text{-}3$$

It is extremely important to recognize that Equations 5-2 and 5-3 lack parameters for fill fraction and vehicle inertia ratio. They also lack terms that relate to the tank shape or internal hardware. This means that T_D must be determined separately for each tank shape and for each combination of fill fraction and effective inertia ratio. Test and flight experience has repeatedly shown that it is not valid to apply Equation 5-3 to combinations of FF and σ_{eff} that differ by more than a few percent from those previously tested or flown.

Sensitivity to fill fraction is apparent when one considers that liquid modes and modal frequencies are affected by the amount of liquid in a tank. The inertia ratio's importance is apparent when one considers that the nutation frequency is a function of the inertia ratio. If the nutation frequency is at or near a liquid modal frequency then resonance can occur. Resonance involves rapid energy dissipation and consequently rapid nutation change. As shown in Section 2.1.2, nutation frequency is related to effective inertia ratio by the following equation:

---

* "Relatively insensitive" means that the parameter has a second or third order effect, not that it has no effect at all. Time constant calculations based on Equations 5-2 and 5-3 should thus be considered approximate rather than exact. See Section 5.1.4 for a discussion of sensitivity to Reynolds number.

† For a given fill fraction, the liquid mass in a tank is proportional to ρr^3 and the moment of inertia about the tank center is proportional to the liquid mass times r^2.

$$\lambda = \Omega \left| \sigma_{eff} - 1 \right| \qquad 5\text{-}4$$

As Equation 5-4 shows, nutation frequency is proportional to vehicle spin rate. This is important because liquid modal frequencies on a spinning vehicle also tend to be proportional to spin rate. Thus, it is usually impossible to escape from a resonance by changing spin rate. According to Equation 5-3, a resonance can be made less severe (i.e., the time constant can be made longer) by reducing the spin rate. However, this is not the same thing as escaping from a resonance.

There are two noteworthy exceptions to the observation that liquid modal frequencies are usually proportional to the vehicle's spin rate. The first exception is for partially filled tanks at very low spin rates. If the spin rate is low enough for surface tension to have significant influence then the liquid distribution within a partially filled tank will be different from the distribution at higher spin rates. This affects the liquid flow pattern, mode shapes, and resonant frequencies. The second exception is for tanks that constrain the liquid within diaphragms or bladders. A diaphragm or bladder's equilibrium shape is governed, in part, by the magnitude of the centrifugal force. In other words, the shape is a function of spin rate. At high and low spin rates, the equilibrium shape may be essentially independent of spin rate. However, for a broad range of intermediate spin rates the diaphragm or bladder shape and liquid modes may have nonlinear dependencies on spin rate.

5.1.2 Applying DTC's from Major-Axis Spinners to Minor-Axis Spinners and Vice Versa

Equation 5-4 reveals a symmetry between major axis spin ($\sigma_{eff} > 1$) and minor axis spin ($\sigma_{eff} < 1$). Specifically, major and minor axis spinners that rotate at the same rate can have the same nutation frequency. For example, vehicles with inertia ratios of 1.3 and 0.7 will have identical nutation frequencies if they have the same spin rate. If the two vehicles also nutate such that their cyclic transverse angular rates have identical amplitudes then any onboard liquids will experience identical excitations and will dissipate energy at the same rate. This symmetry means that the nutation performance of a major axis spinner can be used to predict the performance of a minor axis spinner and vice versa. This does not, however, mean that the two vehicles will have the same dimensionless time constant.

The mathematical relationship between DTC's for major and minor axis spinners can be determined by examining the nutation time constant's dependence on the mean energy dissipation rate. For simplicity, the following mathematical formulation will be based on the assumption that the vehicle is inertially symmetric. In other words, it is assumed that the vehicle's mass properties are equivalent to those of a homogeneous cylinder. For a simple spinner with a nutation amplitude of zero, the kinetic energy (E) and the magnitude of the angular momentum (H) are as follows

$$E = \frac{1}{2} I_S \Omega^2 \qquad 5\text{-}5$$

$$H = I_S \Omega \qquad 5\text{-}6$$

If instead of being in a state of simple spin the vehicle is nutating with a rate about the nominal spin axis of ω_S and a rate about the transverse axis of ω_T then Equations 5-5 and 5-6 become

$$E = \frac{1}{2}\left(I_S\omega_S^2 + I_T\omega_T^2\right) \qquad 5\text{-}7$$

$$H = \sqrt{(I_S\omega_S)^2 + (I_T\omega_T)^2} \qquad 5\text{-}8$$

If there is no externally applied torque, the vehicle's total angular momentum (rigid body plus liquid) will be constant. However, viscous flow within any propellant tanks will cause the kinetic energy to decay, and this will change the relative amplitudes of ω_S and ω_T. If θ is the nutation angle as defined in Section 2.1.5 then the body rates can be expressed as follows:

$$\omega_S = \frac{H}{I_S}\cos(\theta) \qquad 5\text{-}9$$

$$\omega_T = \frac{H}{I_T}\sin(\theta) \qquad 5\text{-}10$$

Substituting these expressions into Equation 5-7 yields the rotational kinetic energy as a function of the angular momentum and nutation amplitude.

$$E = \frac{H^2}{2}\left(\frac{\cos^2(\theta)}{I_S} + \frac{\sin^2(\theta)}{I_T}\right) \qquad 5\text{-}11$$

If the nutation angle is changing with time then the rate of change in kinetic energy is given by

$$\dot{E} = H^2\,\dot{\theta}\sin(\theta)\cos(\theta)\left(\frac{I_S - I_T}{I_S I_T}\right) \qquad 5\text{-}12$$

Because liquid flow in the tanks is cyclic during nutation, the derivatives of both kinetic energy and nutation angle will vary over the nutation cycle. For simplicity, however, the remaining analytical steps will assume that the derivatives represent averages over a nutation cycle rather than instantaneous values.

Most cases of practical interest involve nutation angles of only a few degrees. We can thus make the small angle approximations $\cos(\theta) \approx 1$ and $\sin(\theta) \approx \theta$. Equation 5-12 thus becomes

$$\dot{E} \approx H^2\,\dot{\theta}\,\theta\left(\frac{I_S - I_T}{I_S I_T}\right) \qquad 5\text{-}13$$

Applying the definition of the effective inertia ratio yields

$$\dot{E} \approx H^2\,\dot{\theta}\,\theta\left(\frac{\sigma_{eff} - 1}{I_S}\right) \qquad 5\text{-}14$$

If the nutation angle changes exponentially as described by Equation 5-1 then Equation 5-14 can be expressed as

$$\dot{E} \approx \frac{H^2\theta^2}{\tau}\left(\frac{\sigma_{eff}-1}{I_S}\right) \qquad 5\text{-}15$$

Since the nutation angle is assumed to be small, we can make the additional approximations $\omega_S \approx \Omega$ and $H \approx I_S\Omega$. This leads to

$$\theta \approx \frac{I_T\omega_T}{I_S\Omega} \quad \text{or} \quad \theta \approx \frac{\omega_T}{\sigma_{eff}\Omega} \qquad 5\text{-}16$$

Substituting these approximations into Equation 5-15 yields

$$\dot{E} \approx \frac{(I_S\Omega)^2}{\tau}\left(\frac{\omega_T}{\sigma_{eff}\Omega}\right)^2\left(\frac{\sigma_{eff}-1}{I_S}\right) \qquad 5\text{-}17$$

This can be simplified as

$$\dot{E} \approx \frac{I_S\omega_T^2}{\tau}\left(\frac{\sigma_{eff}-1}{\sigma_{eff}^2}\right) \qquad 5\text{-}18$$

As mentioned at the beginning of this section, if a major-axis spinner and a minor-axis spinner both have the same spin rate, the same nutation frequency, and the same amplitude for the transverse angular rate, then any onboard liquid will dissipate energy at the same rate. If we further assume that the two vehicles have identical spin-axis moments of inertia then Equation 5-18 yields the following

$$\frac{I_S\omega_T^2}{\tau_{major}}\left(\frac{\sigma_{major}-1}{\sigma_{major}^2}\right) = \frac{I_S\omega_T^2}{\tau_{minor}}\left(\frac{\sigma_{minor}-1}{\sigma_{minor}^2}\right) \qquad 5\text{-}19$$

If the spin rates and nutation frequencies of the two vehicles are identical, Equation 5-4 leads to

$$\left(\sigma_{major}-1\right) = -\left(\sigma_{minor}-1\right) \qquad 5\text{-}20$$

Equation 5-19 can thus be reduced to

$$\tau_{major}\sigma_{major}^2 = \tau_{minor}\sigma_{minor}^2 \qquad 5\text{-}21$$

Finally, by applying Equation 5-21 to the definition of the dimensionless time constant we have

$$\boxed{\frac{T_{D\,major}}{T_{D\,minor}} = \left(\frac{\sigma_{minor}}{\sigma_{major}}\right)^2 \quad \text{if} \quad \left(\sigma_{major}-1\right) = \left(1-\sigma_{minor}\right)} \qquad 5\text{-}22$$

With this relationship one can apply nutation time constant data collected from major axis spinners to minor axis spinners and vice versa.

5.1.3 DTC's for Inertially Asymmetric Vehicles

The dimensionless time constants that are presented in this report presume that the vehicle is inertially symmetric. In other words, it is presumed that the vehicle is dynamically equivalent to a homogeneous cylinder. The nature and effect of inertial asymmetry can be understood by considering a vehicle that nominally spins about its Z-axis and that has principal axis inertias I_{XX}, I_{YY}, and I_{ZZ}. The vehicle is considered to be inertially asymmetric if $I_{XX} \neq I_{YY}$. Nutation produces cyclic angular rates (ω_X and ω_Y) about the X and Y-axes, with the rates varying at the nutation frequency and 90° out of phase relative to each other. If we let $\sigma_X = I_{ZZ}/I_{XX}$ and $\sigma_Y = I_{ZZ}/I_{YY}$, and define Ω_X and Ω_Y as the amplitudes of ω_X and ω_Y, we have the following relationship during constant-amplitude nutation.

$$\frac{\Omega_X}{\Omega_Y} = \sqrt{\frac{\sigma_Y - 1}{\sigma_X - 1}} \qquad 5\text{-}23$$

If X is the intermediate moment of inertia axis then σ_X is closer to 1.0 than σ_Y, regardless of whether Z is the major or minor axis. Applying this observation to Eq'n 5-23 yields $\Omega_X > \Omega_Y$ if X is the intermediate axis. In other words, angular motion about the intermediate axis is more vigorous than that about the other transverse axis.

The significance of asymmetric nutational motion becomes clear when one considers that, although the outer shells of virtually all tanks are surfaces of revolution, few propellant tanks are simple hollow spheres. If a non-spherical tank's symmetry axis (the shell's axis of revolution) is not parallel to the vehicle's spin axis, then the tank is considered geometrically asymmetric relative to the transverse axes. In other words, a tank is considered geometrically asymmetric if its projection is different when viewed along the two transverse principal axes. Most tanks, including spherical tanks, have internal geometric asymmetry resulting from the shape and orientation of internal propellant management devices. Partially filled off-axis tanks also have internal geometric asymmetry because centrifugal force causes the liquid to pool in a volume that is asymmetric relative to the two transverse axes. Whether the geometric asymmetry is internal, external, or both, the contained liquid tends to dissipate more energy when the tank is oscillated about one transverse axis then when it is oscillated with the same amplitude about the other transverse axis. As mentioned above, the vehicle's cyclic transverse angular rate is greatest about the intermediate axis. Thus, aligning the tank axis that produces the most vigorous energy dissipation with the vehicle's intermediate axis yields the shortest possible nutation time constant. If the tank is rotated 90° from this worst-case orientation, with the rotation being about an axis parallel to the spin axis, the resulting configuration will have the longest possible time constant for that particular tank and fill fraction. The greater the inertial and geometric asymmetries, the greater the difference between the shortest and longest possible nutation time constants.

Several authors have observed and reported energy dissipation to be predominantly in response to oscillations about the axis that is perpendicular to a tank's axis of geometric symmetry. Although this limited number of observations may not apply universally, they make physical sense. In reporting the results of experimental studies with a sphere-cone tank, Martin (1971b) stated that

> *"...highly energetic fluid motion is excited in a spinning tank when the tank is subjected to angular oscillations (such as those of a nutating spacecraft) about an axis which is not parallel to the tank's symmetry axis. As the angle between these two axes increases (up to 90°), the liquid's motion becomes more violent."*

In other words, Martin's experiments demonstrated that the liquid responded most vigorously to oscillations about an axis that was perpendicular to the tank's symmetry axis. Hubert and Goodzeit (1983) observed a similar phenomenon when comparing flight and test performance of a spherical tank with a flexible internal propellant management device. Specifically, they noted that energy dissipation was dominated by angular motion about the axis that was perpendicular to the PMD's axis of symmetry.

To summarize, Equation 5-23 shows that liquid in a tank on an inertially asymmetric vehicle is driven by unequal angular rates about the two transverse axes. Sensitivity to inertial asymmetry depends on the degree of tank asymmetry and on how much the amplitude ratio in Equation 5-23 deviates from 1. The greater the deviation from 1, the more care must be taken in applying DTC's to configurations that differ from the one for which the data was collected. As a rough rule of thumb, asymmetry should be taken into account if the amplitude ratio in Equation 5-23 deviates from 1 by more than 20%.

Given the great variety of tank configurations, it is impossible to develop a universal DTC correction to account for the interaction between inertial asymmetry and geometric asymmetry. If the vehicle in question has a significant inertial asymmetry and its tank has a significant geometric asymmetry then it may be prudent to test the tank on a platform that accurately models the inertial asymmetry. If that is not possible, the effect of inertial asymmetry can be bounded by a DTC correction that assumes energy dissipation to be entirely due to cyclic angular rates about a single transverse axis. Let σ_{eff} be the effective inertia ratio as defined in Section 2.1.2, and $\sigma_T = I_S/I_T$, where I_S is the spin axis inertia and I_T is the moment of inertia about the transverse axis that is perpendicular to the tank's symmetry axis. The DTC for an inertially asymmetric vehicle can be estimated from that for an inertially symmetric vehicle as follows:

$$DTC_{asymmetric} \approx \left(\frac{1-\sigma_T}{\sigma_T^2}\right)\left(\frac{\sigma_{eff}^2}{1-\sigma_{eff}}\right) DTC_{symmetric} \qquad 5\text{-}24$$

Without explicit testing, it can be unclear whether oscillation about a single tank axis drives most of the energy dissipation. When such an ambiguity exists, Equation 5-24 can be used to calculate worst-case upper and lower bounds for the dimensionless time constant. For a minor-

axis spinner, energy dissipation causes nutation growth and thus the worst-case lower bound on the DTC should be used. This means that for a minor-axis spinner σ_T should be based on the intermediate axis moment of inertia. For a major-axis spinner, energy dissipation is desirable because it causes nutation to damp. Hence, for a major-axis spinner the worst-case time constant should be calculated using a value for σ_T that is based on the minimum moment of inertia.

5.1.4 Sensitivity to Reynolds Number

As mentioned in Section 5.1.1, the dimensionless time constant is in most cases relatively insensitive to Reynolds number; a fact that has been reported by McIntyre (1984), Marcè, et al. (1981), and others. It must be pointed out, however, that relative insensitivity does not mean complete insensitivity. Some of the data collected during this study gives insight into the actual dependence on Reynolds number. For example, Figure 5-1 presents results from air bearing tests of a spherical tank that contained a flexible propellant management device (see Section 6.1.4 for details about this particular tank). The plotted data was collected over a wide range of spin rates for a fill fraction of 1.0 and two different inertia ratios. Since Reynolds number is proportional to nutation frequency, which in turn is proportional to spin rate, the sensitivity to spin rate that is shown in Figure 5-1 is a direct indication of sensitivity to Reynolds number. The DTC normalization represented by Equation 5-2 presumes that the nutation time constant is inversely proportional to the spin rate and that the DTC is thus independent of spin rate. Figure 5-1 shows that although this is a reasonably good approximation, it is not exact.

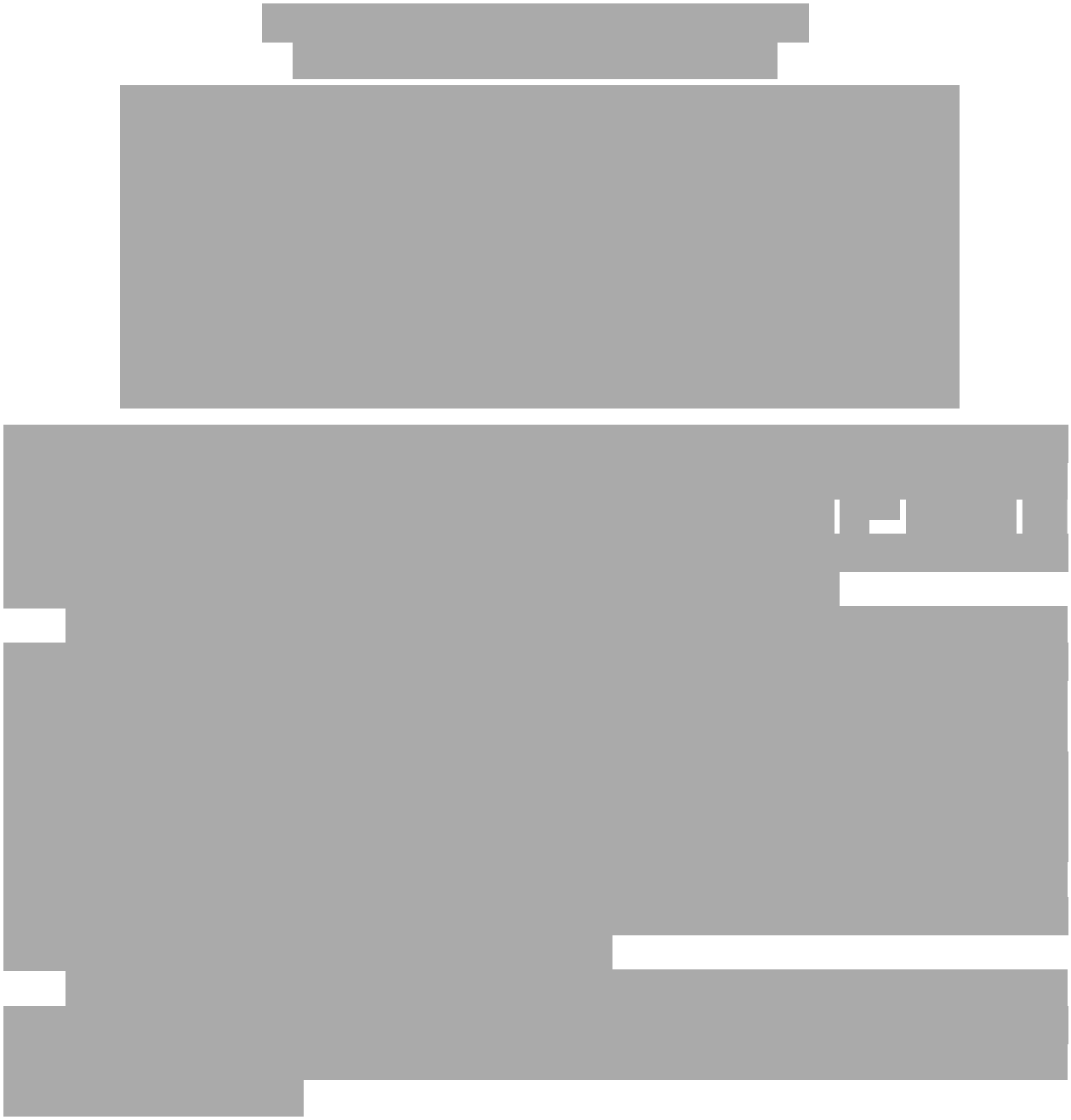

5.1.5 Limitations of the Dimensionless Time Constant

Normalization via the dimensionless time constant is based on the presumption that nutation grows or decays exponentially. If the nutation behavior is not exponential, predictions based on a DTC model are invalid and an alternative normalization method, such as the one described in Section 5.2.3, must be used. Furthermore, as can be seen from scatter in the flight and test data that is presented later in this report and from the discussion of Reynolds number in Section 5.1.4, it is essential to allow for some margin when applying a DTC to a new vehicle configuration. One can expect vehicle-to-vehicle variations even under identical operating conditions. It is thus prudent to apply at least a factor 2 margin to the nutation time constant.

DTC models can be inaccurate if

- DTC's are based on flight or test conditions with long time constants and they are applied to conditions that involve very short time constants (τ <10 nutation cycles). The reverse is also a potential accuracy problem.
- DTC's are based on flight or test conditions in which the liquid is a major fraction of the vehicle's total mass or spin-axis moment of inertia (>20%) and they are being applied to conditions in which the liquid represents only a small fraction of the vehicle's mass or inertia. The reverse is also a potential accuracy problem.
- The Bond number* is less than 10 (unless DTC data is collected and applied to conditions with essentially the same Bond number).
- The Froude number† is less than 10 (unless DTC data is collected and applied to conditions with essentially the same Froude number or if the tank is 100% full).
- The vehicle's moments of inertia are highly asymmetric; unless DTC data is collected and applied to conditions with essentially the same degree of asymmetry and the tanks have similar physical locations and orientations relative to the asymmetry. For more about this see the discussion in Section 5.1.3.

5.1.6 Spinning Vehicles with Tanks of More Than One Type

If a vehicle is to be flown with tanks of more than one type, its divergent nutation time constant can be determined by first calculating the time constant that each tank would yield on its own and then combining the effects of all tanks. If we represent the net time constant due to all tanks with the symbol τ_{NET} and represent the independent time constant for each tank as τ_1, τ_2, τ_3, etc., then the relationship between the time constants is

$$\frac{1}{\tau_{NET}} = \frac{1}{\tau_1} + \frac{1}{\tau_2} + \frac{1}{\tau_3} + \cdots \qquad 5\text{-}24$$

As Equation 5-24 shows, it is a simple matter to determine the net time constant from the individual contributions of each tank. It is more difficult to do the reverse. If nutation data is collected from a test or flight vehicle, and if the vehicle has more than one tank type, it is usually impossible to determine the individual contributions of each tank. An exception is for configurations in which DTC data is independently available for all but one of the tank types. In

* The ratio of inertial force (e.g. centrifugal force) to surface tension force at the liquid's free surface.

† The ratio of centrifugal force to axial force at the free surface. The Froude number is essentially infinite during simple spin but can be low when the vehicle is thrusting or during some types of ground-based testing.

that circumstance, Equation 5-24 can be used to determine the remaining tank's contribution to the time constant.

5.1.7 Sensitivity to Tank Volume (Designs with a Single Tank vs. Multiple Tanks)

If two tanks have the same shape and fill fraction but different volumes, the larger tank will dissipate more kinetic energy and thus produce a shorter nutation time constant. Furthermore, the fractional decrease in NTC is greater than the fractional increase in liquid mass. For a given tank shape and fill fraction, the tank volume and contained liquid mass are proportional to the tank radius cubed (r^3). The nutation time constant is inversely proportional to the liquid's self-inertia, which is proportional to the liquid mass times the tank radius squared. The NTC is thus inversely proportional to r^5 (Equation 5-3). The relationship between the nutation time constant (τ) and the tank volume (V) is thus

$$\tau \propto \frac{1}{V^{5/3}} \qquad 5\text{-}25$$

As a numerical example, consider two tanks of the same shape that are both 90% full. If one tank has twice the volume as the other, its nutation time constant will be shorter by a factor of 3.17. If the only design consideration is to maximize the NTC, it would be better to double the volume by adding a tank than to increase the size of the tank.

If multiple tanks all have the same size, shape, and fill fraction, then from Equation 5-24 we see that τ_{NET} equals the time constant for a single tank divided by the number of tanks. If the propellant load is doubled by doubling the number of tanks, the nutation time constant will be reduced by a factor of 2. This is better than the factor of 3.17 NTC reduction that results from doubling the propellant load by doubling the tank volume. If there is a need to maximize the nutation time constant, it is better to use multiple small tanks than a single large tank. For a given net tank volume (sum of all tanks), the relationship between the NTC and the number of tanks (N) is given by the following equation.

$$\tau_{NET} \propto N^{2/3} \text{ (for a constant net tank volume)} \qquad 5\text{-}26$$

Equation 5-26 assumes that all tanks have the same shape and fill fraction. If two smaller tanks replace a single large tank, the nutation time constant is increased by 59%. If three smaller tanks are used, the net NTC is more than double that of a single tank with the same net volume.

5.1.8 Determining the Nutation Time Constant from Flight or Drop Test Data

Figure 5-2 is a plot of accelerometer data from a typical subscale drop test in which nutation grows exponentially. This data can be analyzed in several ways to determine the time constant. The simplest method is to determine the peak-to-peak amplitude of the accelerometer output for each nutation cycle and to calculate the rate at which that amplitude grows. In other words, the time constant is determined by examining the envelope of the nutation data.

Envelope methods are often best when data is sparse, such as the Lunar Prospector sun sensor data shown in Figure 5-3. On the other hand, if digital data is available with a sampling

rate that is at least an order of magnitude greater than the nutation frequency, other methods can more accurately quantify the nutation performance. For this study, digital data was typically analyzed using a least-squares fit to an exponentially growing or decaying sinusoid. Approaches of this type can yield very accurate measurements of both the nutation time constant and the nutation frequency. If the spin rate is accurately known then the nutation frequency can be used to determine the apparent inertia ratio (Section 2.1.4).

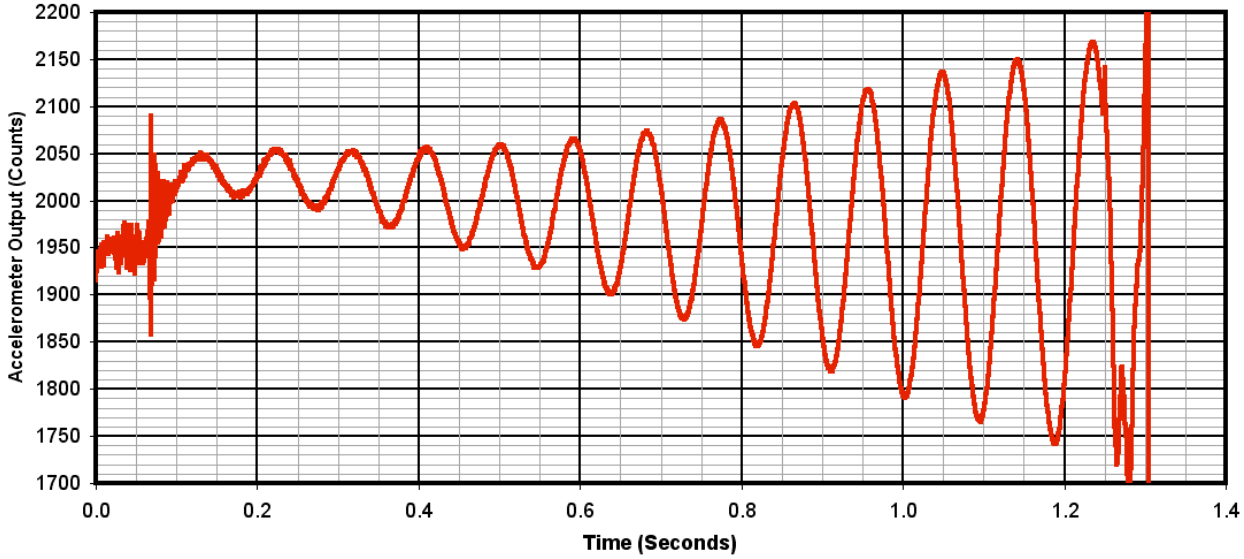

Figure 5-2 Drop Test Data Showing Exponential Nutation Growth

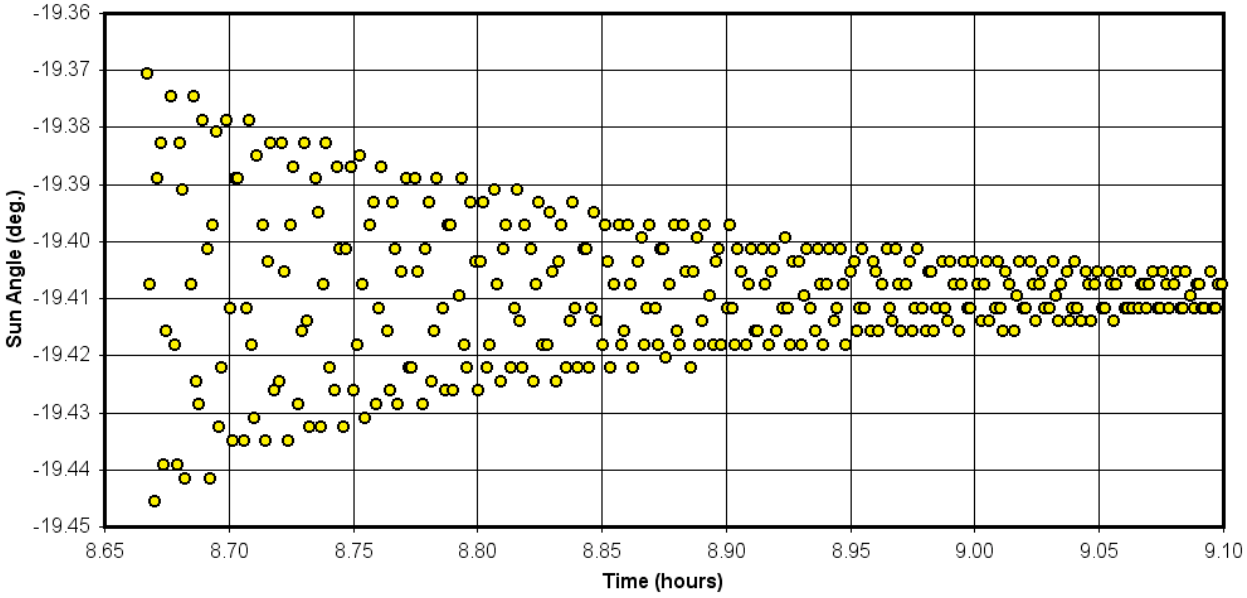

Figure 5-3 Lunar Prospector Sun Sensor Data Showing Exponential Nutation Decay

5.1.9 Dimensionless Time Constants from Forced Motion Tests

It is straightforward to use Equation 5-2 to compute a dimensionless time constant from drop test or flight data. All needed parameters values are directly available. On the other hand, forced

motion tests (Section 4.4.4) involve constrained motion. Since there is no nutation growth, a nutation time constant cannot be directly measured. Furthermore, "spin-axis moment of inertia" has no real meaning for forced motion testing.

Fortunately, as described below, the ratio τ/I_S can readily be computed from forced motion test data. The computation, however, involves an implicit assumption that linear energy dissipation mechanisms predominate. This assumption cannot be confirmed from test data because forced motion testing is usually done at only one nutation amplitude. Fortunately, drop tests and flight performance indicate that most tank configurations involve linear behavior. With a linear energy dissipation mechanism, the relationship between the nutation time constant and the mean energy dissipation rate is given by Equation 5-27.

$$\tau = \theta^2 \left(\frac{I_S \Omega^2}{P} \right) \left(1 - \sigma_{eff} \right) \qquad 5\text{-}27$$

Here, θ is the nutation angle as defined in Section 2.1.5, and P is the mean energy dissipation rate (average over a nutation cycle). This formulation involves an implicit assumption that the NTC is at least an order of magnitude larger than the nutation period. From Equation 2-18, the effective inertia ratio for a minor-axis spinner is related to the spin rate (Ω) and nutation frequency (λ) as follows.

$$\sigma_{eff} = 1 - \frac{\lambda}{\Omega} \qquad 5\text{-}28$$

Equation 5-28 can be used to determine the effective inertia ratio of a forced motion test. Assuming small amplitude nutation, the effective nutation angle for the test is a function of the spin rate and the amplitude of the cyclic transverse rate (Ω_T).

$$\theta = \frac{\Omega_T}{\Omega \sigma_{eff}} \qquad 5\text{-}29$$

Substitution of 5-28 and 5-29 into 5-27 and rearranging yields

$$\frac{\tau}{I_S} = \frac{\Omega \Omega_T^2 \lambda}{\left(\Omega - \lambda \right)^2 P} \qquad 5\text{-}30$$

Substituting 5-30 into 5-2 yields an expression for the DTC that is appropriate for use with forced motion test data.

$$T_D = N \left(\frac{\rho r^5 \lambda}{P} \right) \left(\frac{\Omega \Omega_T}{\Omega - \lambda} \right)^2 \qquad 5\text{-}31$$

The mean energy dissipation rate, P, is the work done during one nutation cycle divided by the nutation period. An example of how to determine this will be given for the current Spinning Spacecraft Test Rig (SSTR) at the Southwest Research Institute. On this rig, the test tank is

supported by three load cells. The combined output of these cells is used to compute net 3-axis forces and torques about the midpoint of the load cell cluster. If we denote the force vector as $\underline{F}_{TEST}$, the torque vector as $\underline{T}_{TEST}$, the vector from the rig's center of rotation to the centroid of the load cell cluster as $\underline{R}_{TEST}$, and the tank's angular velocity vector as $\underline{\omega}_{TEST}$, then the mean energy dissipation rate is given by Equation 5-32.

$$P = \frac{\lambda}{2\pi}\int_0^{2\pi/\lambda}\left(\underline{R}_{TEST}\times\underline{F}_{TEST}+\underline{T}_{TEST}\right)\bullet\underline{\omega}_{TEST}\,dt \qquad 5\text{-}32$$

If the load cells support a simple rigid body with no internal dissipation mechanisms, the integral will be zero. For tests that involve liquid in a tank, a non-zero integral reflects energy dissipation by viscosity effects. The combination of Equations 5-31 and 5-32 allows forced motion test data to be normalized using the dimensionless time constant method.

5.2 Non-Exponential Nutation Change

Several conditions can cause nutation sensor data profiles to be non-exponential. These include the excitation of other transient phenomena and nonlinear damping.

5.2.1 Identifying Resonant Conditions From Beating Between Nutation & Liquid Modes

During subscale drop tests it is not unusual for the release transient to excite one or more liquid modes with frequencies that differ from the nutation frequency. The resulting attitude motion yields non-exponential nutation sensor outputs such as that in Figure 5-4, which has a clearly visible beating between an exponentially growing nutation and an exponentially decaying liquid mode. Behavior of this type is most likely to occur when a liquid modal frequency is near but not identical to the nutation frequency. Although this type of behavior can occur in flight on spinning vehicles that are subject to large transients, such as engine burns and separation events, the phenomenon is usually much more subtle in flight than that shown in Figure 5-4.

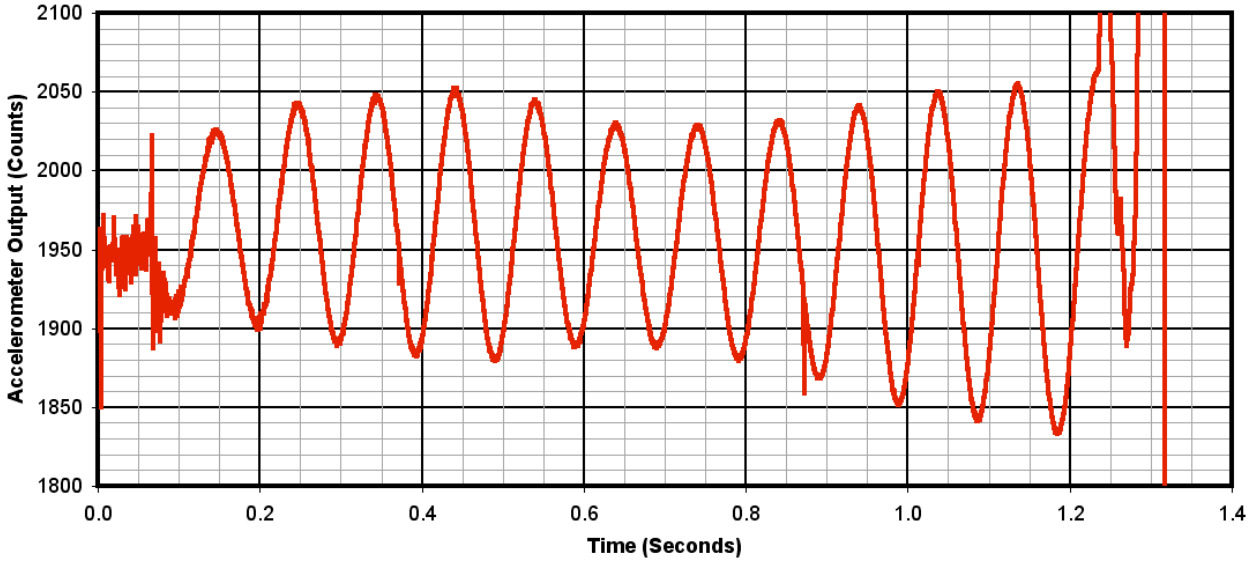

Figure 5-4 Drop Test Data Showing Beating Between Nutation and a Liquid Mode

To determine a dimensionless nutation time constant using data of the type shown in Figure 5-4 it is necessary to mathematically separate nutation from other components of the signal. Although fast Fourier transforms are often used to determine the frequency components of a complex signal, FFT's are inappropriate when the component amplitudes are rapidly changing. Furthermore, even if FFT's can isolate frequencies, they will not yield time constants. An additional problem with FFT's is that accurate determination of a given frequency requires a data set with a large number of cycles. For example, to determine the nutation frequency to an accuracy of ±1% requires at least 50 nutation cycles of data. Applying an FFT to the drop test data shown in Figure 5-4 would yield a nutation frequency with an uncertainty of about 5%. This is not good enough to accurately identify resonant conditions. Hence, an alternative approach is needed.

For this study, behavior of the type shown in Figure 5-4 was analyzed using least squares fits to functions with multiple exponentially changing sinusoids. This approach yields frequencies *and* time constants, and only a few cycles of data are needed for accurate frequency measurements. The extracted non-nutation frequencies are the result of liquid motion, and these frequencies can be used to identify resonant conditions without those specific conditions being tested or flown. Resonance exists when the nutation frequency matches a liquid modal frequency. Hence, to find a resonance one can simply use Equation 5-4 to determine the effective inertia ratio that yields a nutation frequency equal to the extracted liquid modal frequency. In doing this, it is important to remember that liquid modal frequencies are usually proportional to the vehicle's spin rate. Hence, resonant conditions are identified by solving Equation 5-4 for effective inertia ratio; not for spin rate.

Although the process described in the previous paragraph can be used to identify conditions that cause resonance, it cannot be used to determine the divergent nutation time constant at that resonance. The time constant can only be determined via testing or from flight data at the resonance. Despite that limitation, knowledge that a resonance exists is valuable because it lets vehicle designers know what conditions to avoid or, if a resonance is unavoidable, gives designers a heads-up that further testing is required and that a robust active nutation control system may be needed.

5.2.2 Nutation Synchronous Motion

As described in Section 3.1, nutation synchronous motion can occur if the vehicle's spin axis passes through a partially filled tank. Once a nutation synchronous mode is fully established the energy dissipation rate due to liquid motion is essentially independent of the nutation amplitude, provided the nutation angle is less than about 10 deg. In other words, kinetic energy loss is more like that from Coulomb friction than from viscous friction.

From Equation 5-14 it can be seen that if we let C_1 be the constant rate of change of energy, then the differential equation for the nutation angle is

$$\dot{\theta}\theta \approx \frac{C_1 I_S}{H^2\left(\sigma_{eff} - 1\right)} \qquad 5\text{-}33$$

This equation has the solution

$$\theta \approx \sqrt{\frac{C_1 I_S t}{H^2\left(\sigma_{eff} - 1\right)} + C_2} \qquad 5\text{-}34$$

where C_2 is a constant of integration. Note that because kinetic energy is dissipated from the system, C_1 is negative. Figure 5-5 shows a nutation profile in which an initial exponential growth ($t < 0.3$ sec) transitions into nutation synchronous motion ($t > 0.4$ sec). In this example, the transition to nutation synchronous motion occurred at a nutation angle of approximately 2 degrees. Note that nutation grows more slowly once the mode transition is complete.

Because nutation does not change exponentially during nutation-synchronous motion, it is not valid to normalize the behavior using a dimensionless time constant. An alternative normalization technique must be applied.

5.2.3 Dimensionless Energy Dissipation Rate

In addition to introducing the dimensionless time constant scaling described in Section 5.1.1, Neer and Salvatore (1972) introduced a related energy dissipation scaling concept, which they referred to as a "dimensionless energy group." The Neer-Salvatore scaling method is used here in slightly modified form as the *dimensionless energy dissipation rate,* β. This parameter is mathematically defined by

$$\beta = \frac{-\dot{E}}{N\rho r^5 \Omega^3 \theta^2} \qquad 5\text{-}35$$

Because viscosity effects cause kinetic energy to be lost, β is always positive. Using Equation 5-14 to substitute for the energy dissipation rate we can, after some rearrangement, express the dimensionless energy dissipation rate in terms of the nutation growth rate.

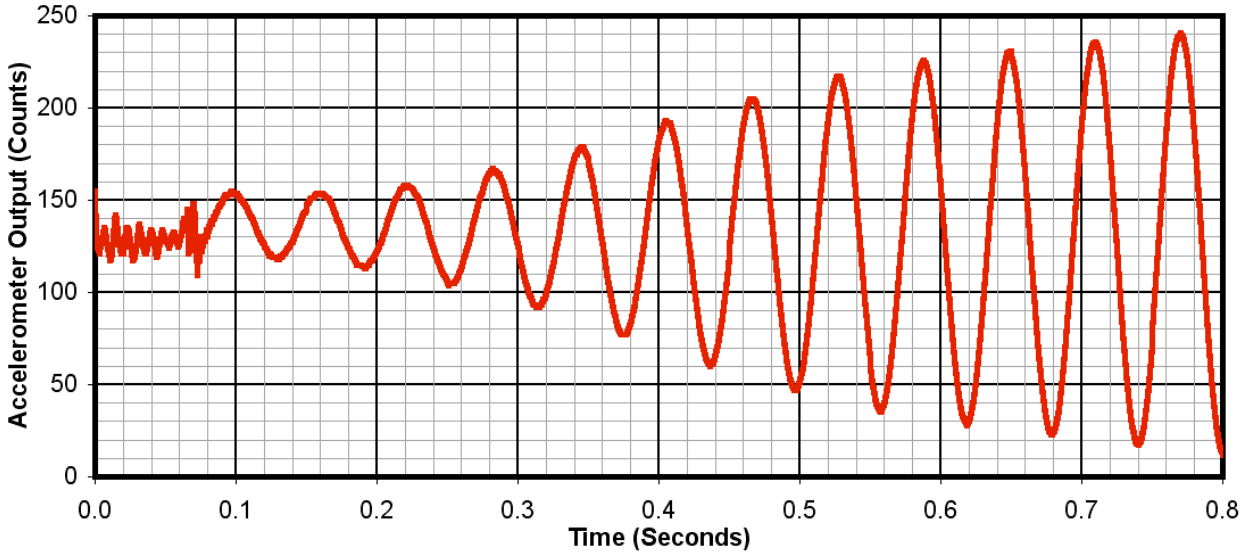

Figure 5-5 Drop Test Data Showing Transition to Nutation Synchronous Motion

$$\beta = \left(\frac{I_S}{\rho r^5}\right)\left(\frac{1-\sigma_{eff}}{N\Omega}\right)\frac{\dot{\theta}}{\theta} \qquad 5\text{-}36$$

If β is known, the rate of change of the nutation angle can be calculated from

$$\dot{\theta} = \left(\frac{\rho r^5}{I_S}\right)\left(\frac{N\beta\Omega}{1-\sigma_{eff}}\right)\theta \qquad 5\text{-}37$$

Equations 5-36 and 5-37 apply to all energy dissipation mechanisms; linear and nonlinear. If the energy dissipation mechanism is linear (i.e., if the nutation angle changes exponentially) we can simply the formulation by applying the relationship between the nutation angle and its derivative.

$$\frac{\dot{\theta}}{\theta} = \frac{1}{\tau} \qquad 5\text{-}38$$

Here, τ is the nutation time constant. Substituting Equation 5-38 into Equation 5-36 yields

$$\beta = \left(\frac{I_S}{\rho r^5}\right)\left(\frac{1-\sigma_{eff}}{N\Omega\tau}\right) \qquad 5\text{-}39$$

Applying the definition of dimensionless time constant from Equation 5-2 yields the relationship between the dimensionless time constant and the dimensionless energy dissipation rate.

$$\beta T_D = 1 - \sigma_{eff} \qquad 5\text{-}40$$

Note that Equations 5-39 and 5-40 are independent of θ and apply only to exponential nutation change. If the nutation angle changes non-exponentially, such as when a nutation-synchronous mode is active, β is a function of θ and must be evaluated using Equation 5-36.

5.3 Cautions and Limitations

The scaling methods described above can be used to predict the behavior of vehicles that have not yet flown. However, when doing this one must keep in mind that liquid resonances can be quite sharp and small parameter changes can thus result in very different behaviors. Scaling is valid only if the vehicle being analyzed is sufficiently close to previously tested or flown combinations of dimensionless parameters. The critical parameter space includes vehicle inertia ratio, tank shape, tank fill fraction, tank location relative to the vehicle center of mass, propellant management device shape and stiffness, etc. Interpolation between closely spaced data points is acceptable, but extrapolation outside the range of available flight or test data can be risky. This report discusses many instances in which small changes in fill fraction or inertia ratio yield large changes in the dimensionless time constant.

As a rule of thumb, one should not extrapolate to fill fractions that are more than 5% beyond the range of existing flight or test data points. Similarly, extrapolation should not be done to effective inertia ratios that cause $|\sigma_{eff} - 1|$ to deviate by more than 5% from the nearest

value for existing data. This inertia ratio constraint is derived from nutation frequency considerations (see Equation 5-4). For most cases of practical interest, the nutation frequency and the liquid modal frequencies are essentially proportional to the vehicle's spin rate. In other words, the ratio of nutation frequency to liquid frequency is independent of spin rate. If this frequency ratio is 1.0, resonance exists and rapid nutation change will result. By applying a 5% constraint on $|\sigma_{eff} - 1|$ we are, in effect, applying a 5% constraint on the difference between the nutation/liquid frequency ratio for the configuration being analyzed and the nutation/liquid frequency ratio for the existing data.

Note that the inertia ratio constraint becomes more stringent as the effective inertia ratio gets closer to 1.0. For example, if test data is collected at an effective inertia ratio of 0.20 then it should be a good indicator of performance for inertia ratios ranging from 0.16 to 0.24, or ±4.0%. However, if data is collected at an inertia ratio of 0.80, its applicability is limited to the relatively narrow range of 0.79 to 0.81, or ±1.25%.

5.4 Mass Properties Uncertainties

Determining the most appropriate way to model the mass properties of liquids on a spinning vehicle is a persistent unresolved issue, and the lack of a good theory has led to a multiplicity of approaches being used. Although the problem cannot be completely untangled, some understanding can be gained by considering the ways in which mass properties are actually used. Dynamic analysis of spinning vehicles involves two distinct classes of problems; one requiring accurate knowledge of the spin-axis moment of inertia and the other requiring accurate knowledge of the inertia ratio. Unfortunately, each class of problems makes different demands on the mass properties model.

5.4.1 Momentum-Sensitive Dynamics

This class of problems involves determining the time and propellant required to change the direction or magnitude of the vehicle's total angular momentum vector relative to inertial space (e.g., attitude precession or spin rate change). This requires accurate knowledge of the vehicle's total angular momentum, which in turn requires accurate knowledge of the spin-axis moment of inertia. To achieve the desired accuracy requires modeling the propellant moments of inertia as if the liquids were frozen where they would be when the vehicle is in a simple, steady-state spin about its nominal spin axis. Ideally, this includes modeling the curved free surface. This class of problems is relatively insensitive to uncertainties in the inertia ratio.

5.4.2 Nutation-Sensitive Dynamics

These problems involve determining nutation damping or de-damping performance, attitude behavior during orbital maneuvers, and spin-axis stability. This requires accurate knowledge of the inertia ratio but is less sensitive to uncertainties in the absolute moments of inertia. For this class of problems, liquid motion causes the nutation frequency and the stability boundaries to be different than would be predicted with a frozen-liquid model. This type of problem requires not actual moments of inertia but *apparent* moments of inertia. In other words, what is needed are

the moments of inertia of an equivalent solid vehicle that has the same nutation frequency as the actual vehicle. The nutation frequency is a key parameter because it provides a fundamental measure of spin-axis stability. Instability occurs when the nutation frequency becomes zero (i.e., when the *apparent* inertia ratio is 1.0).

5.4.3 Modeling Methods

At one time or another, all of the following models have been used to calculate the contributions of liquid propellants to vehicle mass properties.

1. *Cylindrical free surface* – For a centerline tank, this is the best model of the actual location of the liquid during simple spin with no nutation.
2. *Truncated sphere or cylinder* – For a tank that is offset from the spin axis, this is the best model of the actual location of the liquid during simple spin with no nutation. Although the free surface is generally considered to be flat, rather than curved, this is the most mathematically complex of the frequently used models.
3. *Completely filled tank* – With this simple model, the density of the liquid is adjusted to be consistent with the total liquid mass.
4. *Central bubble* – This model assumes a central spherical void equal to the ullage volume. Although this model may have some justification for a non-spinning vehicle, it does not represent the distribution of liquid in a tank that is mounted on a spinner.
5. *Point mass at the liquid center of mass* – This model places a point mass at the liquid's nominal c.m. location during simple spin with no nutation. If the tank dimensions are small relative to the distance between the tank center and the spin axis, this model produces results that are close to those of truncated sphere or cylinder models.
6. *Point mass at the center of the tank* – The simplest of all the models, this approach is usually used only as a first approximation.

For an off-axis tank, the truncated model clearly provides the most accurate approximation of the vehicle's angular momentum as a function of spin rate. It's thus the best model for the momentum-sensitive dynamic analyses discussed above. Flight and drop test data, however, suggest that truncated tank models can lead to inaccurate predictions of the vehicle's nutation frequency. In other words, the model that works best for momentum-sensitive dynamic analyses is a poor model for nutation-sensitive dynamics analyses. This is a particular concern for estimates of the apparent inertia ratio; which is an important measure of the vehicle's dynamic stability margin and an important factor in determining the nutation time constant.

Flight performance suggests that for spherical tanks without diaphragms or bladders the liquid's self-inertia is largely decoupled from the vehicle's nutational motion and that, for nutation-sensitive dynamic analyses, the liquid in an off-axis spherical tank is best represented by the simplest of all models for mass properties calculation: a point mass located at the tank's

center. Unfortunately, there is insufficient information to determine how to best model the liquid in other types of tank. It is probably best to calculate the vehicle mass properties using several different liquid models and to use the differences in the resulting inertia ratios as a measure of the liquid's contribution to uncertainty in that parameter. Remember that this uncertainty must be added to uncertainty in the vehicle's dry inertia ratio, which is typically 3% at launch and can be 10% or more during the vehicle's preliminary design.

6. Spherical Tanks

Spherical tanks have been extensively used on spinning vehicles and experience has shown that simple spheres with little or no internal hardware cause relatively slow nutation change if they are offset from the vehicle's spin axis. However, bare tanks that are mounted on the spin axis can cause rapid nutation growth if the system has the wrong combination of fill fraction and inertia ratio. For both on-axis and off-axis tanks, internal hardware increases energy dissipation, sometimes dramatically. The first known report of such behavior was by Reiter and Lee (1966). Their subscale tests of the centerline spherical tank for the Able-5 Lunar mission showed that dividing the tank into cubical compartments produced nutation growth rates that could have led to mission failure. In their KC-135 ballistic trajectory tests, baffles produced growth rates equivalent to a divergent nutation time constant of 4 to 5 seconds at the 170-rpm operational spin rate. Their tests also showed that without baffles nutation growth was negligible; a result that was subsequently confirmed by mission telemetry. A more extensive series of tests by Vanyo and Likins (1973) investigated baffles in the form of an array of parallel square tubes. Although these baffles reduced energy dissipation relative to an unbaffled tank for effective inertia ratios close to 1.0, they significantly increased energy dissipation at ratios below 0.88 to 0.80, depending on the dimensions of the squares. Vanyo and Likins attributed the increased energy dissipation to turbulence and cautioned against indiscriminate use of untested baffles.

A similar result was found in air bearing tests of a spherical tank with and without an internal propellant management device. These tests showed that, for a completely filled tank, the PMD decreased the divergent nutation time constant by a factor of 15 [Hubert and Goodzeit, 1983]. A few years later, an extensive series of forced motion tests of the INSAT-1 spacecraft showed significant sensitivity to PMD design. For the range of designs tested, energy dissipation varied by nearly an order of magnitude [Garg, et al., 1986].

Test and flight performance have repeatedly shown that internal hardware can have a profound effect on the rate at which energy is dissipated by a liquid propellant. If a PMD is highly flexible, even a large device may have only a moderate effect on energy dissipation. On the other hand, relatively small pieces of rigid hardware can have a surprisingly large effect.

6.1 Off-Axis Spherical Tanks

6.1.1 Off-Axis Tanks with no Internal Hardware

An off-axis spherical tank with no internal hardware appears at first glance to be a relatively simple energy dissipation mechanism. This simplicity is deceptive. When mounted on a nutating vehicle, these tanks exhibit fluid flow with a complexity that has thus far confounded purely analytical efforts to accurately predict nutation time constants. As will be seen in this subsection, simple spherical tanks yield dimensionless time constants that can vary by , depending on the combination of fill fraction and vehicle inertia ratio.

6.1.4 Off-Axis Tanks with Flexible Propellant Management Devices

Figure 6.1-12 illustrates a spherical tank that was used on several early commercial communications satellites. The propellant management device included a set of thin surface tension vanes for use during non-spinning operations. These flexible vanes were attached to the tank at only two points. Specifically, they were welded in place at the outlet and pinned at a point directly opposite the outlet. The pin was free to rotate about the tank's axis of symmetry. Elsewhere there was a small clearance between the vanes and the tank wall.

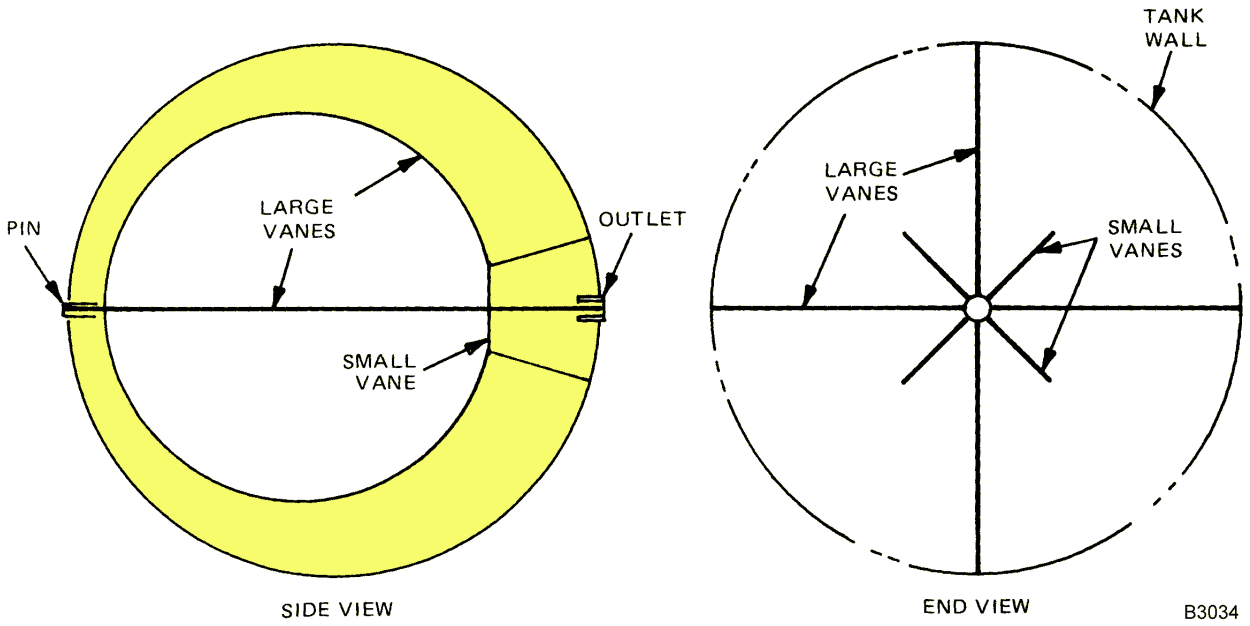

Figure 6.1-12. Spherical Tank with Flexible Surface Tension Vanes

Hubert and Goodzeit (1983) presented the results of full-scale air bearing tests and some flight performance data for the tank described above. They also presented air bearing test results for the same size tank without a PMD. These tests demonstrated that liquid interaction with the PMD was the dominant energy dissipation mechanism, and that this interaction decreased the nutation time constant by a factor of 15 relative to a bare tank.

7. Sphere-Cone Tanks

An excellent example of a non-spherical configuration that is susceptible to inertial waves is the sphere-cone tank. As seen in Fig. 7-1, a sphere-cone tank with a large fill fraction has a free surface that is the same as that of a simple spherical tank. Furthermore, at high fill fractions the free-surface sloshing characteristics are nearly the same in the two types of tanks. Below the surface, however, the deviation from spherical has been shown to excite vigorous liquid motion.

Because sphere-cone tanks have been used on numerous spinning and dual-spin spacecraft, they have been extensively tested. At Comsat, a plexiglass sphere-cone tank was tested on a spinning, forced-motion fixture [Martin, 1971]. Turbulent motion was observed in the tank when it was subjected to angular motions similar to those of a nutating spacecraft. The liquid motion was almost entirely subsurface; only a slight dimpling of the free surface could be seen (Fig. 7-1). A spherical tank subjected to the same test conditions showed no such turbulence. There was also no observable turbulence during tests in which the sphere-cone tank was angularly oscillated about its symmetry axis. These tests strongly suggest that angularly oscillating a tank about an axis that is not an axis of symmetry can produce significant energy dissipation.

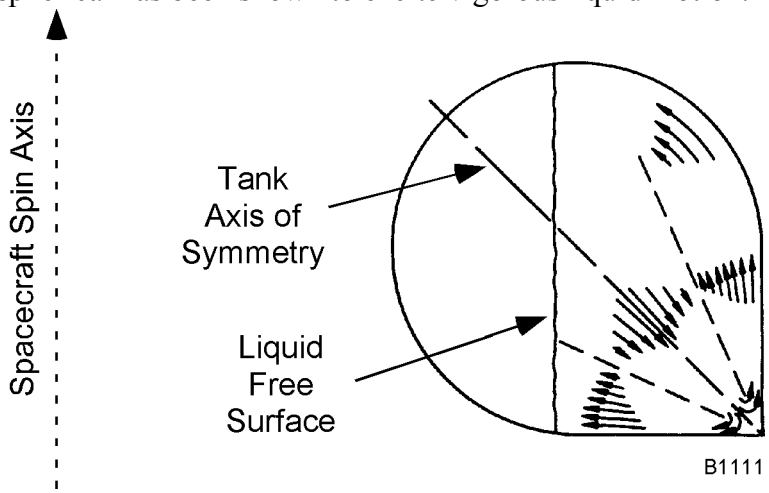

Figure 7-1. Flow within a sphere-cone tank (adapted from Fig. 7 in Martin 1971)

In-orbit tests of Intelsat IV, which had sphere-cone tanks, showed peak nutation de-damping when the nutation frequency was about one-third of the free-surface sloshing frequency that was measured in preflight ground tests [Slabinski, 1978]. Subsequent ground tests showed similar energy dissipation behavior and showed that the motions involved little or no surface wave activity. The in-orbit tests involved tank fill fractions ranging from 51% to 82%. At each fill fraction, there were two de-damping peaks, neither of which occurred at the free-surface sloshing frequency. At these peaks, the divergent nutation time constant was more than an order of magnitude shorter than at other nutation frequencies. This type of behavior cannot be predicted using analytical models that are based solely on surface-wave sloshing.

Figure 7-2 clearly shows how the divergent nutation time constant for sphere-cone tanks is extremely sensitive to variations in fill fraction and inertia ratio. For example, at a fill fraction of 0.4, the divergent time constant varies from roughly an hour at an inertia ratio of 0.523 down to about 150 sec. at an inertia ratio of 0.461. The strong parameter sensitivities in this figure shows

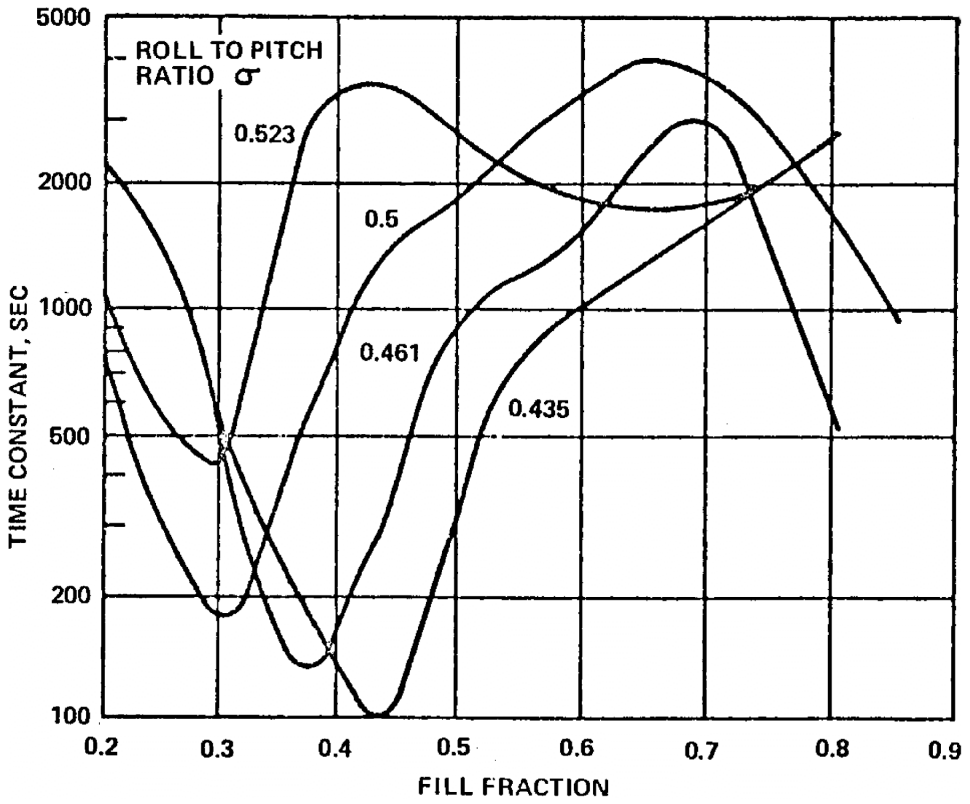

Figure 7-2. Time constant for GOES-D transfer orbit configuration (from McIntyre 1984)

yet again why it is risky to extrapolate test and flight data to operating conditions that are outside the parameter space covered by available data. Additional test and flight data for these tanks is given by Agrawal and James (1981).

Although there has been extensive testing of these tanks, most of the results are proprietary. Furthermore, the data that is publicly available is incomplete and cannot readily be used to compute dimensionless time constants. This lack of information, however, is of no concern because although sphere-cone tanks were widely used two decades ago, they appear to have fallen out of favor. The author is aware of no recent or future vehicle designs that incorporate tanks of this type.

8. Spheroidal Tanks

A spheroid is a figure generated by rotating an ellipse about one of its axes. Tanks of this shape have seldom been used on spinning vehicles. Thus, only limited data is available. Tests by Vanyo (1984) demonstrated that even small deviations from spherical can significantly increase energy dissipation within a completely filled tank. Unfortunately, from the perspective of the current study, Vanyo's experiments were aimed at examining the rotational dynamics of Earth's liquid core and his published results are limited to conditions that correspond to effective inertia ratios between 0.96 and 1.04. Inertia ratios in this range are usually considered unacceptable for spinning space vehicles. A much wider range of inertia ratios was analytically treated by McIntyre and Tanner (1987). Their fluid dynamics analysis of a completely full on-axis prolate spheroid with a height-to-diameter ratio of 2.0 indicated rapid nutation growth at inertia ratios between 0.4 and 0.8. Analysis of their numerical results yields a very low dimensionless time constant of 0.09 at inertia ratios near 0.6. Unfortunately, McIntyre and Tanner presented no test data to confirm these results. The current study was able to uncover only two limited data sets that are relevant to the use of oblate spheroidal tanks on spinning space vehicles, and none for prolate spheroids.

9. Cylinders and Tanks with Cylindrical Sections

9.1 Cylindrical Tanks

Extensive study of spinning spacecraft and liquid-filled artillery shells with cylindrical tanks uncovered dramatic rotational instabilities, principally due to inertial waves [Scott and D'Amico, 1973; D'Amico, 1974; McIntyre and Tanner, 1987; Selmi and Herbert, 1995]. The observed resonances can be sharp, with a 10% difference in vehicle inertia ratio leading to an order of magnitude difference in the nutation time constant. Severe resonances have been observed in both completely filled and partially filled cylindrical containers. Tests of on-axis cylindrical tanks have also shown that the liquid resonant frequency can be amplitude-dependent. Data published by Scott and D'Amico (1973) show a 20% or more difference in the resonant frequency for small and large amplitude nutation, where the transition to "large" amplitude occurs at between 1 and 8 degrees. The author of the current study, however, is unaware of any actual or planned use of cylindrical tanks on spinning space vehicles.

9.5 Off-Axis with Cylindrical Midsection, Hemispherical Ends, and Baffles

Off-axis tanks with cylindrical midsections and hemispherical ends have exhibited severe nutation problems involving both resonant and non-resonant behavior. This type of tank often requires baffles to suppress rapid nutation growth.

9.5.1 Need for Baffles and Evaluation of Baffle Types

Eurostar was the first vehicle to be tested with tanks that had cylindrical midsections and hemispherical ends. The spacecraft was originally planned for Shuttle launch with a spinning solid upper stage. Although the launch vehicle was later changed to Ariane after the Challenger accident, extensive drop testing was conducted to determine the effect of liquid propellants on the nutation behavior of the spacecraft while mounted on a spinning upper stage. The tested tank† is shown in Fig. 9.5-1. There were four of these tanks: two containing monomethyl hydrazine and two containing nitrogen tetroxide. All four had their centers offset from the spin axis by 2.06 times the tank radius and all four had their long axes parallel to the spin axis.‡

As reported by Pocha (1984, 1987), initial subscale drop tests indicated a full-scale divergent time constant of 24 sec. for mass properties that corresponded to the configuration before the third stage's solid engine burn and 33 sec. for the post-burn configuration, both at 30 rpm. These values were unacceptable. Follow-up tests showed that performance of the pre-burn configuration (inertia ratio 0.44) was sensitive to the amount of liquid in the tanks, with the nutation time constant for completely filled tanks being less than half that seen when the tanks were 75% full. On the other hand, tests of the post-burn configuration (inertia ratio 0.61)

---

*

† The tested PMD (Fig. 9.5-1) is slightly different from the one that was actually flown. Specifically, the flight and test tanks had the small cylindrical "sponge" in different locations. The flight design is PSI Part Number 80310-5. A data sheet can be found at www.psi-pci.com.

‡ A drawing of the tank layout can be found in Pocha (1987).

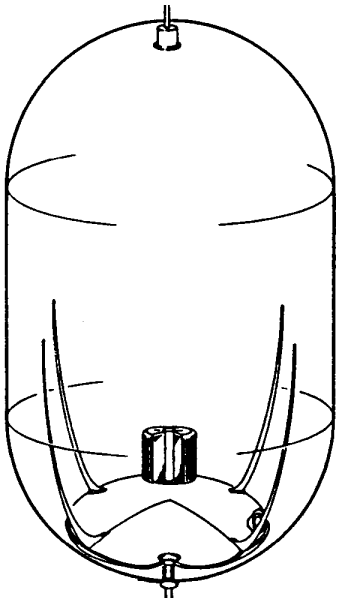

Fig. 9.5-1 Eurostar Tank (from Pocha 1987)

showed nutation performance to be relatively insensitive to fill fraction over a relatively wide range: 0.5 to 1.0. Furthermore, at a fill fraction of 0.89, nutation performance was relatively insensitive to inertia ratio over a range of 0.55 to 0.68. The pre-burn sensitivity to fill fraction suggests that the vehicle parameters were at or near a resonance. The post-burn insensitivity to parameter variation suggests that its short time constant may have been more the result of bulk fluid motion than a response to a liquid mode.

Subsequent testing showed that a significant portion of the energy dissipation was due to flow past the four slender flexible surface tension vanes. Although removing the vanes roughly doubled the pre-burn and post-burn divergent time constants, the performance was still unacceptable. Several slosh baffle designs were then tried (Figure 9.5-2) and it was found that an annular baffle (marked "A" in the figure) could improve the divergent nutation time constants by an order of magnitude. Best performance was achieved with the baffle mounted in the center of the tank (measured in the long direction) and with a width that was half the tank's inside radius. The baffles marked "B" and "C" proved to be much less effective. This suggests that the original nutation problem was caused by interaction with a liquid mode that had flow parallel to the tank's long axis but with no significant rotational flow about the long axis.

Unfortunately, there is insufficient published data to map out dimensionless time constants for the Eurostar tank. Nevertheless, the information about baffle configurations that do and do not work is extremely valuable, and the next subsection presents test results for a tank with a nearly identical aspect ratio and offset from the spin axis.

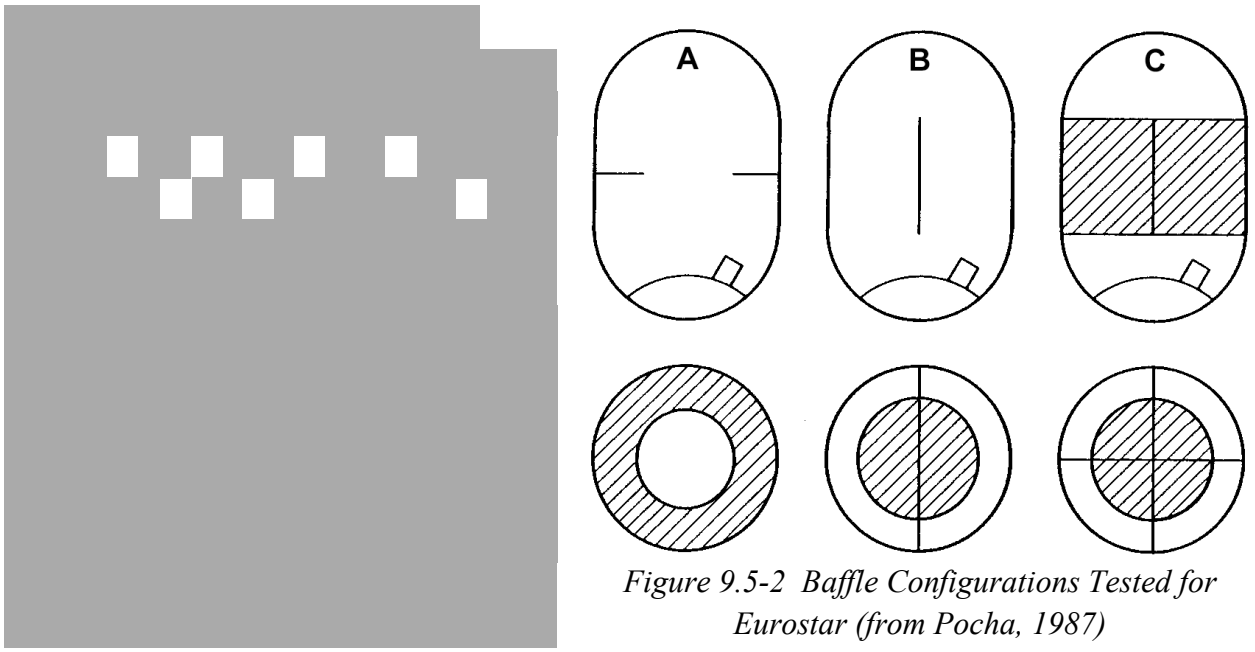

Figure 9.5-2 Baffle Configurations Tested for Eurostar (from Pocha, 1987)

10. Tanks with Diaphragms or Bladders

Diaphragms and bladders are elastic barriers that separate liquid propellants from the pressurant gas. A diaphragm is essentially a flexible wall. In a diaphragm tank the contained liquid is in direct contact with both the flexible barrier and the portion of the tank's rigid wall that is on the propellant side of the diaphragm. In a bladder tank the propellant is entirely within a flexible inner container and the tank's rigid walls are not wetted.

10.1 Asymmetry in Diaphragm and Bladder Tanks

In diaphragm and bladder tanks, the flexible barrier causes the liquid to be within an asymmetric compartment unless the tank is loaded to capacity. This asymmetry is a consequence of the elastic barrier being able to bend much more easily than it stretches, which causes the barrier's surface area to be essentially independent of the amount of liquid in the tank. The effect of nearly constant surface area on shape is illustrated in Figure 10.1-1. Furthermore, unless the diaphragm is fully distended, a multiplicity of equilibrium shapes are possible, as can be seen in the photographs in Figure 10.1-2. Having liquid within an asymmetric container of uncertain shape has several consequences for energy dissipation and the resulting nutation change. The most obvious effect is that surface wave mode shapes and modal frequencies will be more sensitive to fill fraction than in a tank without a diaphragm or bladder. Furthermore, if a surface wave is excited, hysteresis associated with cyclic bending will significantly increase modal damping. Depending on circumstances, this increased damping could so suppress the surface wave that nutation change is slowed, or it could dramatically increase the energy dissipation at resonance. The latter effect is more likely to occur if the tank is far from the vehicle's center of mass and thus subject to greater cyclic acceleration. Asymmetry also raises the possibility that subsurface inertial waves may be excited. This must always be considered when liquid is contained within a non-spherical compartment. As with surface modes, subsurface inertial wave frequencies and mode shapes may depend strongly on the diaphragm or bladder shape, and thus on the fill fraction. Finally, energy dissipation from bulk fluid motion is affected by the liquid's "free" surface being in contact with an elastic solid instead of a gas because viscous drag is increased as the fluid moves past the wrinkled surface.

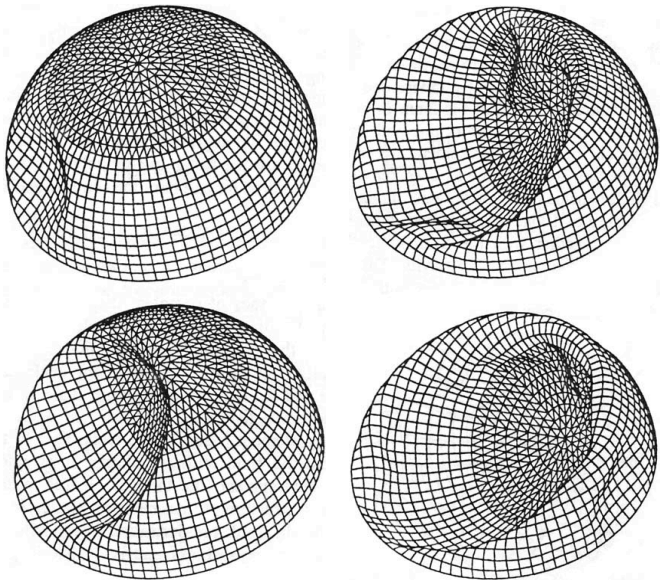

Figure 10.1-1. Typical Diaphragm Shape at Different Fill Fractions [from Kreis, et al., 1996]

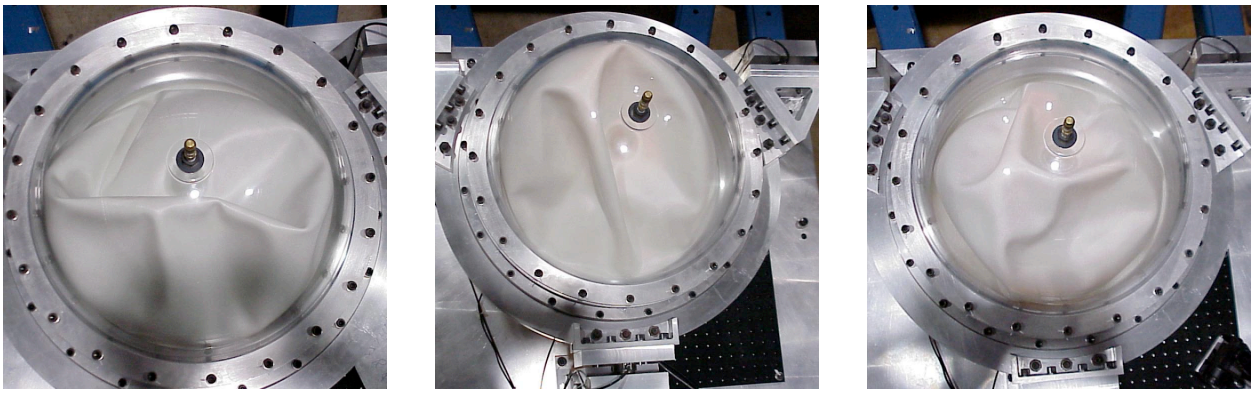

Figure 10.1-2 Examples of diaphragm equilibrium shapes in a 71% full tank (photographs courtesy Southwest Research Institute)

Using test and flight data to predict the performance of other vehicles with "identical" diaphragms or bladders is complicated by uncertainties associated with non-repeatability in wall thickness and variations in equilibrium shape. Due to variability in the molding process, diaphragm and bladder thickness can vary from sample to sample and from different locations on the same diaphragm or bladder. This variability holds for both subscale test tanks and full-scale flight tanks. Furthermore, the number and shape of dimples and wrinkles in a diaphragm or bladder may depend on the sequence of events that preceded the spinning operation of interest, with uncertainty in the shape being greatest for an on-axis tank (Section 10.4). Variations in these and other parameters may shift a liquid resonance so that it occurs at a somewhat different fill fraction or inertia ratio than previous tests or flight data might indicate. Because of this, some conservatism must be used when applying the results of this section.

10.3.2 On-Axis with Diaphragm Parallel to Spin Axis

The EXOSAT spacecraft had a single 48.41 cm (19.06 in.) diameter nearly spherical on-axis hydrazine tank with a diaphragm and two 31.8 cm (12.5 inch) diameter off-axis spherical propane tanks with no internal hardware. The hydrazine tank was identical to that used on Dawn (Section 10.3.1), but had a different orientation. Specifically, the EXOSAT tank had its diaphragm attachment plane parallel to the spin axis instead of perpendicular to the spin as was the case for Dawn. EXOSAT's two tank types were separately tested at full scale in a CNES air bearing facility to determine the nutation behavior when the spacecraft was mounted on a spinning upper stage. Test results were published in a detailed report by Marcè, Torres, Assemat, and Michel (1981). The diaphragm tank performance is discussed in this section and the propane tank is treated in Section 6.1.1.

The CNES air bearing tests used the same diaphragm as the flight tank (PSI part number 80274-1), but the titanium pressure vessel was replaced with a Plexiglas sphere so that the diaphragm could be observed. Water, which has fluid properties nearly identical to those of hydrazine, was used as the working fluid. The tank was mounted on the test rig to match the position and orientation in flight. Specifically, the spin-axis passed through the center of the tank and the diaphragm's attachment plane was parallel to the spin axis. EXOSAT's nominal spin rate was 50 rpm while attached to the solid propellant upper stage. The inertia ratio ranges

covered by the test program were 0.25 to 0.29 for the stage's pre-burn configuration and 0.31 to 0.38 for the post-burn configuration.

As discussed in Section 4.4, terrestrial air bearing rigs cannot achieve a high Froude number for on-axis tanks. For the EXOSAT tank, this meant that the diaphragm did not assume the same shape that it would in flight. Figure 10.3-7 shows a cross-section of the tank in the test rig. This figure is based on a sketch in the report by Marcè, et al., which in turn was based on direct observation of the diaphragm. Although the sagging seen in Figure 10.3-7 may not represent the diaphragm's true in-orbit shape it is the best that could be done in the air-bearing tests. Note, however, that there is some similarity between the shape in Figure 10.3-7 and those shown in Figures 10.1-1 and 10.4-1. Hence, there may still have been a reasonable degree of realism in the test conditions.

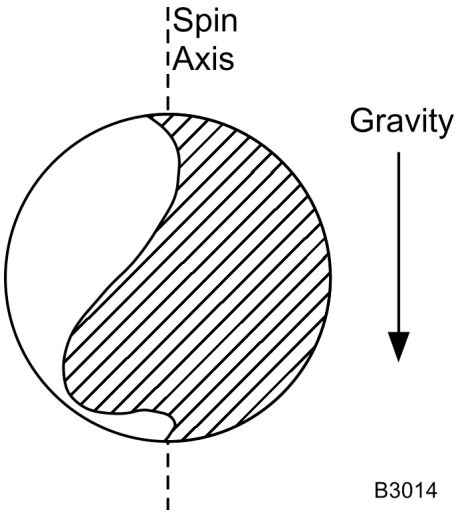

Figure 10.3-7. Diaphragm Sag under the Influence of Gravity

Figure 10.3-8 plots dimensionless time constants that were derived from the air bearing results tabulated by Marcè, et al. The figure shows both raw data points and quadratic curve fits for each fill fraction that was tested. The curves clearly show that the DTC is sensitive to both inertia ratio and fill fraction. Note that the highest tested fill fraction, 0.75, represents the tank's advertised maximum capacity.

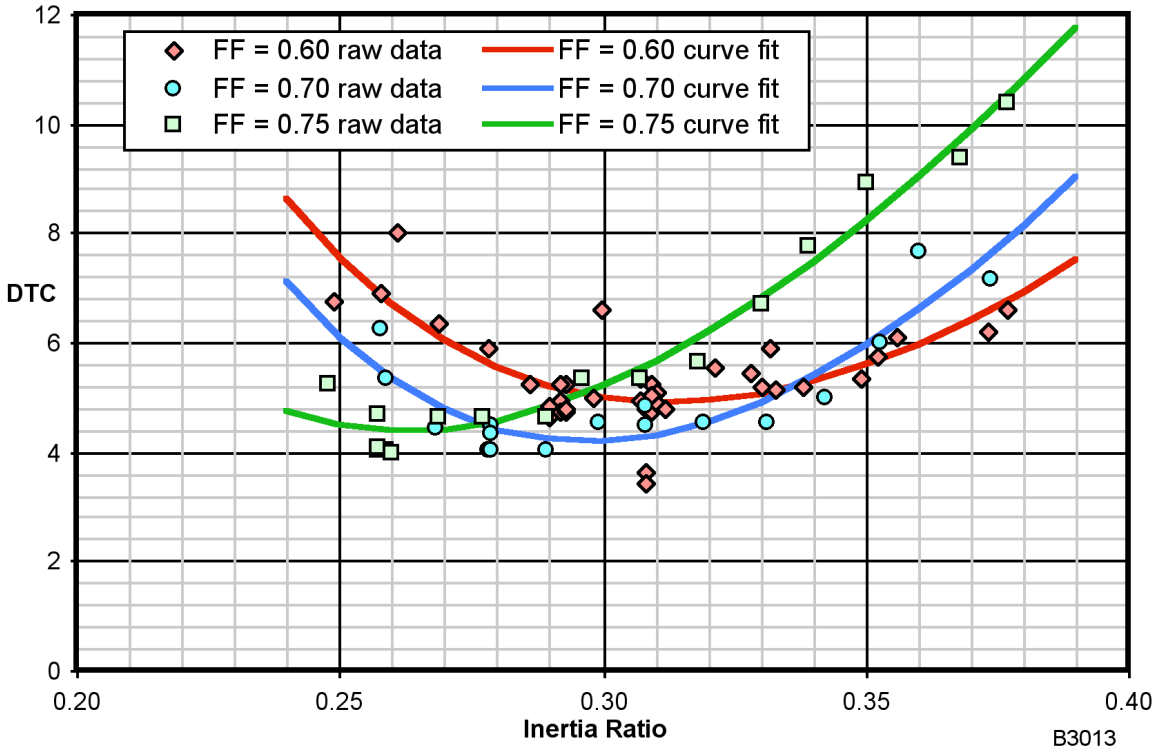

Figure 10.3-8. Dimensionless Time Constants for the EXOSAT Diaphragm Tank

Because the tests were conducted in a 1-g environment, the diaphragm always sagged as shown in Figure 10.3-7, with the degree of sagging depending on the test rig's spin rate. To assess the effect of diaphragm shape, some tests were run at a 0.75 fill fraction with the hydrazine tank displaced 30 cm (11.8 inches) from the spin axis. This displacement introduced a centrifugal force that increased the Froude number and that held the diaphragm closer to its flight orientation. The faster the spin, the closer the diaphragm was to the flight configuration. Although the test results with an offset tank generally agreed with those for an on-axis tank, the nutation time constant became longer as the diaphragm surface got closer to being parallel to the spin axis. For the range of conditions tested, the time constant doubled at inertia ratios near 0.30 and increased by about 60% for inertia ratios near 0.35. This suggests that the DTC's in Figure 10.3-8 are conservatively low, an observation that appears to have been borne out by flight performance.

Marcè, Torres, Assemat, and Michel reported that the tests showed no significant surface wave motion. They thus concluded that energy was dissipated primarily by subsurface flow rather than by flexing of the diaphragm. They also concluded that subsurface motion becomes more vigorous as the configuration becomes less symmetric. In other words, the diaphragm's main effect is on the shape of the liquid-filled cavity, and relatively little energy is dissipated by diaphragm flexing.

According to Marcè, et al., the air bearing tests predicted a worst-case divergent nutation time constant (combined effects of the propane and hydrazine tanks) of 2.5 minutes before the upper stage burn and 1.9 minutes after burnout, with most of the energy being dissipated in the hydrazine tank. These time constants included a 1.5 factor of safety, meaning that the predicted time constants were actually 3.8 and 2.9 minutes, respectively. Although the flight nutation time constant does not appear to have been published, the EXOSAT flight performance was briefly discussed during the 1984 INTELSAT/ESA Symposium on the Dynamic Effects of Liquids on Spacecraft Attitude Control in Washington, DC. EXOSAT was not explicitly covered in any of the papers at the symposium. However, I recorded in my notes a remark by Jean-Pierre Guibert of ONERA that EXOSAT's flight time constant was 400 sec. vs. a 120 sec. worst-case prediction from air-bearing tests. If this worst-case prediction included the same 1.5 factor of safety used by Marcè, et al., the nominally predicted time constant was about 180 sec. Hence, the actual time constant was roughly double that predicted by air bearing tests. This is consistent with the expectation that diaphragm sag caused the air-bearing test results to be somewhat conservative.

The EXOSAT diaphragm tank test program concluded with a series of runs to test for sensitivity to Reynolds number. For these runs, the working liquid was a glycerol-water mixture with twice the viscosity of the pure water used in the other runs. The results confirmed that the nutation time constant is relatively insensitive to viscosity. The same tests also confirmed that the time constant is inversely proportional to the liquid's density. These results are consistent with the normalization approach that underlies the dimensionless time constants used in this report (Section 5.1).

11. Miscellaneous Tank Shapes

11.1 Cylindrical Tank With Ellipsoidal Ends and a Common Ellipsoidal Bulkhead

During the 1980's, Hughes Aircraft Co. considered, tested, and rejected a design in which a single on-axis tank was split into two compartments: one for fuel, the other for oxidizer (Figure 11-1). Subscale drop tests showed that this configuration produced extremely short divergent nutation time constants when the nutation angles was less than about 3 deg, and much longer time constants at higher nutation angles (Fig. 11-2). Subsequent analytical treatment of the problem by McIntyre and Tanner (1987) confirmed that the observed rapid nutation growth was due to inertial waves within the tank.

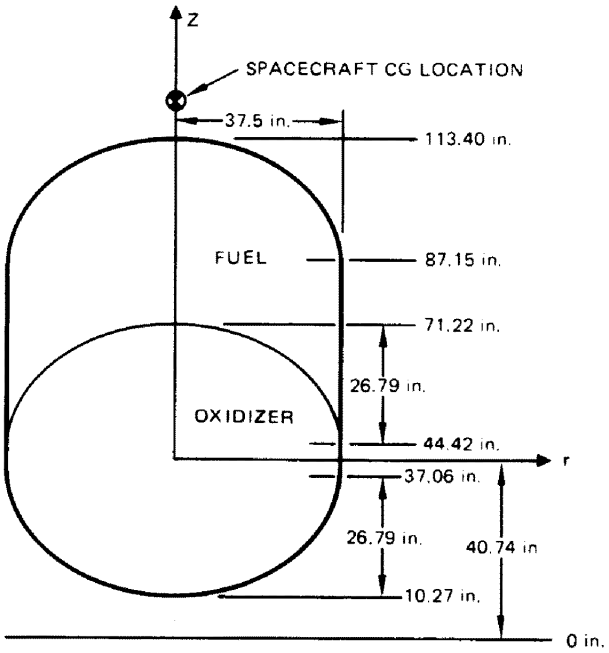

Fig.11-1 Tank with Common Bulkhead (from McIntyre & Tanner 1987)

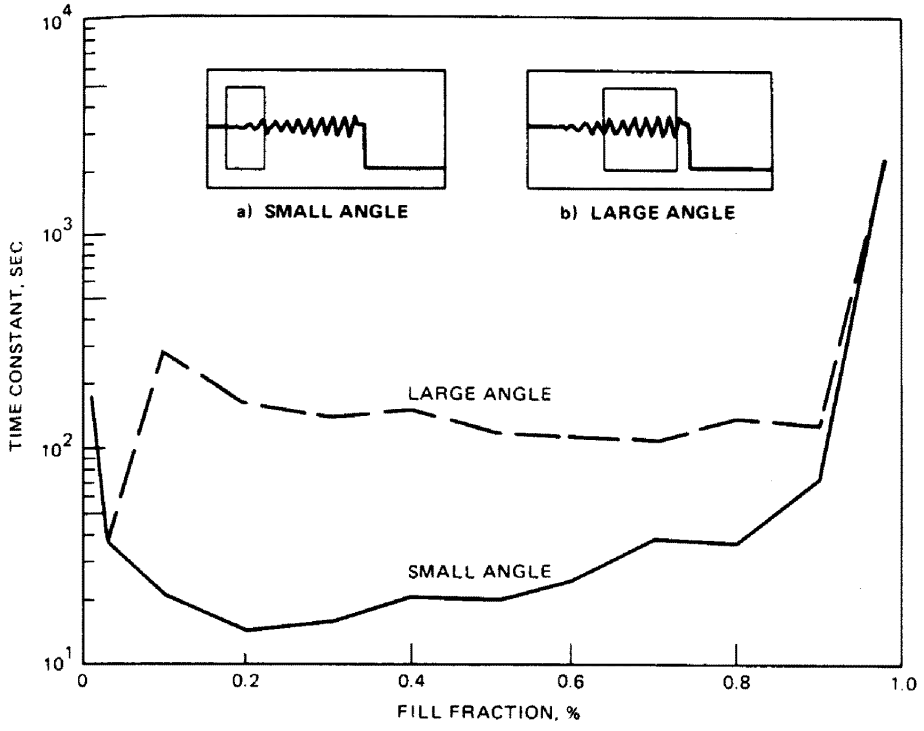

Fig. 11-2 Drop Test Results for Fig. 11-1 Tank (from McIntyre & Tanner; 1987)

11.2 Hemispherical Tanks

In an investigation related to the EXOSAT program, a series of air-bearing tests was run with a 100% full hemispherical tank. In these tests, the tank's flat surface was parallel to the test rig's nominal spin axis. Although this tank shape is unlikely to be used in a space vehicle, it is worth mentioning because it clearly demonstrates that a free surface is not a prerequisite for a resonance involving liquid modes and nutational motion. Figure 11-3 is a plot of test results that were tabulated by Marcè, et al. (1981) for both on-axis and off-axis tanks. The figure shows sharp resonances near inertia ratios of 0.27 and 0.33 and even sharper anti-resonances near inertia ratios of 0.30 and 0.35. Marcè, et al. pointed out that the resonance behavior qualitatively matched the inertial wave modes reported by Greenspan (1969) for a completely filled spherical tank. It is clear that this behavior cannot be predicted or modeled using the simple equivalent pendulums that are often applied to the liquid "slosh" problem.

Another noteworthy characteristic of the data plotted in Figure 11-3 is the consistency between results from the on-axis and off-axis tank tests. This consistency demonstrates that Froude number is irrelevant when a tank is at or very close to 100% full.

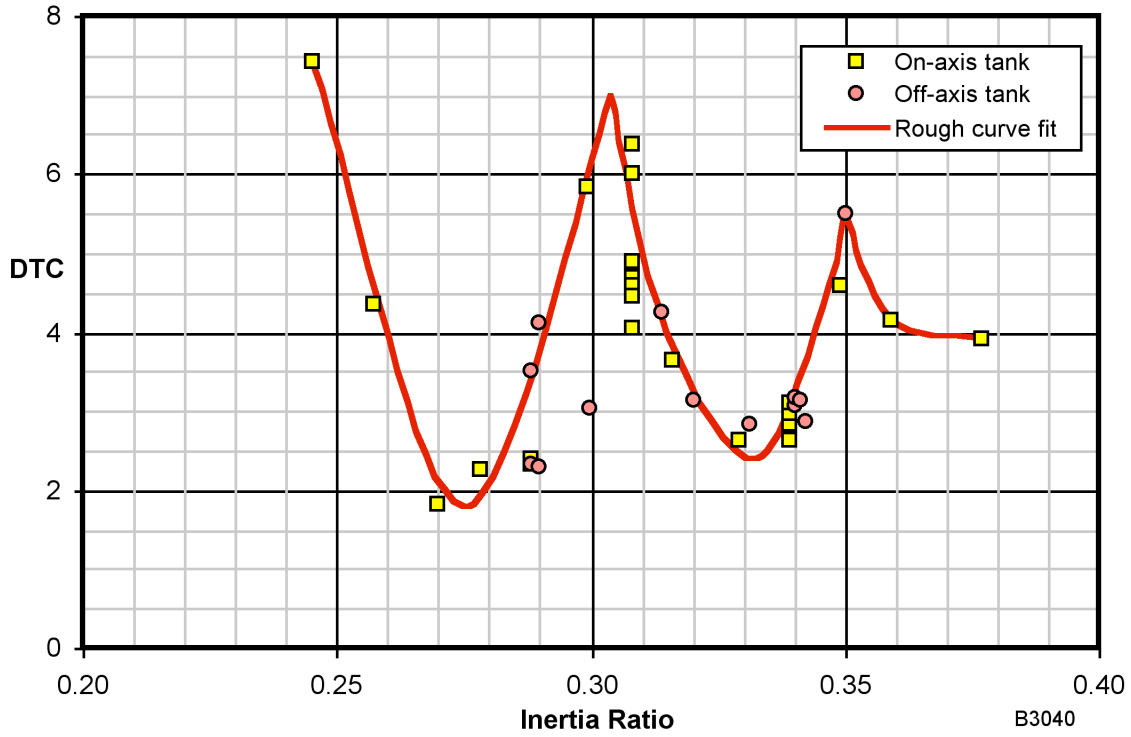

Figure 11-3. Dimensionless time constant for a 100% full hemispherical tank

12. The Analytical Challenge

Each of the several methods for modeling the motion of liquid propellant on a spinning vehicle has significant limitations. The obvious high-fidelity approach is to use a liquid dynamics software package such as FLOW-3D. This method, however, has several shortcomings. First, it is complex and time consuming. Second, there are anecdotal reports that some fluid flow packages do not model Coriolis effects properly, which limits the accuracy in modeling inertial waves on a spinning vehicle. Third, if the propellant management device is flexible, its bending can have a significant influence on the liquid behavior and must be modeled. Most packages cannot easily model the coupled interaction between fluid flow and the flexing of surface tension vanes, diaphragms, or bladders. Fourth, fluid flow packages do not model the effect that the liquid has on the vehicle's six degree-of-freedom motion. In other words, the analytical model mathematically decouples what is in reality a highly coupled system. Finally, fluid flow models tend to be least accurate in their modeling of turbulent drag effects, and it is the energy dissipation associated with drag that is usually of greatest concern. From these observations, it is unclear whether any existing software package can accurately quantify the effect of liquid motion on a vehicle's nutational dynamics.

Mechanical analogs are a commonly used alternative to detailed fluid modeling. A significant advantage of this approach is that it can easily be incorporated into an attitude control simulation or other software package with full coupling between the "liquid" motion and the vehicle's rotational dynamics. The main problem is that a single simple analog cannot emulate all aspects of the propellant motion. The best that can be done is to select a model that emulates the dominant behavior, which leads to the question of what is the dominant behavior. Is it free-surface sloshing, bulk fluid motion, or a subsurface vortex mode? This question is difficult to answer without testing. An even more difficult issue is how one selects values for key parameters. Choosing correct values for the analog's natural frequency and damping rate is a particularly thorny problem if there is no test or flight data available.

Small-amplitude free-surface sloshing is often represented by a simple pendulum with a massless rod and a bob that is a point mass. For an off-axis tank the pendulum's natural frequency is typically well above the nutation frequency.* On the other hand, bulk fluid motion in a partially filled off-axis tank may be best modeled as a short pendulum with a substantial self-inertia. This pendulum's natural frequency is very low — well below nutation frequency. Because free-surface sloshing typically has a "high" frequency and bulk motion has a "low" frequency, a single simple pendulum model cannot adequately emulate both behaviors. The pendulum modeling problem is even more complex if the spin axis passes through the tank. In a

*

centerline tank, the surface wave behavior of greatest concern is often the nutation synchronous mode, in which the liquid swirls around the tank in a single direction at nutation frequency. In this type of motion, the modal mass is a function of nutation amplitude. This is difficult to model with a simple pendulum. Finally, for both on-axis and off-axis tanks, the most severe limitation of pendulum models is that they cannot emulate subsurface inertial waves.

In the extreme, a full or nearly full tank may best be modeled using one or more wheels coupled to the vehicle body by viscous friction and possibly tortional springs. In this situation, there is no free surface and thus no slosh mode. Nevertheless, test and flight experience has shown that substantial energy dissipation is possible in a completely full tank. Whether bulk fluid motion is modeled as a pendulum or a wheel, the damping rate depends almost entirely on the internal hardware configuration. Once again, there is no good analytical method for determining a propellant management device's effect on damping rate without test or flight data.

Perhaps the biggest challenge is to adequately model the behavior of liquids in tanks with diaphragms or bladders. As discussed in Section 10.4, nutation characteristics are strongly influenced by a diaphragm's equilibrium shape. If the diaphragm is not fully distended, it typically has more than one possible equilibrium shape, especially if the tank is located on or near the vehicle's spin axis.

To the author's knowledge, reliable mechanical analogs have yet to be developed that emulate the complexity of vortex modes. One possibility is to use multiple wheels that are coupled to the vehicle's rotational motion with springs and viscous dampers. Once again, there is the difficulty of how one selects the appropriate parameters for such an analog. Complicating the problem is the fact that some configurations have multiple modes, each mode with a different frequency and flow pattern.

Experience shows that it is possible to construct an equivalent mechanical model that accurately emulates observed test or flight behavior. The challenge is in developing a model that accurately *predicts* performance. Simulations that incorporate equivalent mechanical models of onboard liquids will accurately emulate nutation behavior *only if the model and its parameters are based on test or flight data.* The behavior of a nutating vehicle with onboard liquids cannot be predicted using a purely analytical model that has no flight or test data behind it.

13. Future Needs

Although data presented in this report covers a wide range of parameter combinations, it is clear that there remain broad gaps in the data. Figures 13-1 through 13-6 show, for the most commonly used tank types, those combinations of fill fraction and effective inertia ratio for which test or flight data exist. Spherical non-diaphragm tanks are covered by Figures 13-1 and 13-2. Non-diaphragm tanks with cylindrical midsections and hemispherical ends are covered in Figures 13-3 and 13-4. Finally, Figures 13-5 and 13-6 cover tanks with diaphragms.

As Sections 6 through 11 of this report show, nutation performance can be very sensitive to small variations in fill fraction or inertia ratio. Hence, dimensionless time constants should be considered valid only for parameter combinations with fill fractions and normalized nutation frequencies that are within 5% of those combinations for which data actually exists. (Normalized nutation frequency is the nutation frequency divided by the spin rate, and equals 1.0 minus the effective inertia ratio.) As Figures 13-1 through 13-6 show, broad parameter ranges remain uncovered by usable data. Fortunately, many of the uncovered areas are irrelevant to launches with spinning upper stages. The great majority of launches involve fill fractions that exceed 0.5 and effective inertia ratios that are between 0.15 and 0.60. Thus, the area of greatest interest occupies less than a quarter of the parameter space. However, even within this limited range of interest, there are still sizable gaps in the knowledge base.

Based on apparent trends in propulsion system design, the most immediate need is to expand the knowledge base for tanks with diaphragms and bladders. Tests and flight experience have shown strong sensitivity to diaphragm equilibrium shape, although the characteristics and degree of sensitivity have yet to be fully identified. Performance characteristics have been determined for a limited number of tank aspect ratios, and a limited number of diaphragm and bladder designs, but there is still much that is unknown and clear patterns of behavior have yet to emerge. Additional testing is recommended, with particular emphasis on understanding the sensitivity to diaphragm equilibrium shape. Toward this end, it is essential that all future testing of diaphragms and bladders be conducted using tanks with at least one optically clear segment.

The next most important configuration for which better knowledge is needed is the non-diaphragm tank with cylindrical mid sections and hemispherical ends. The available data has enabled a rough mapping of two different resonances.

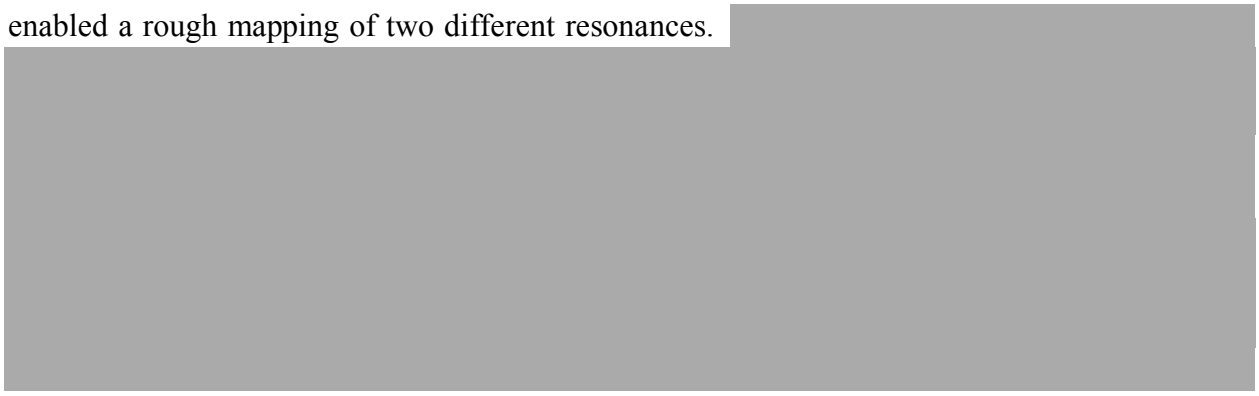

Spherical non-diaphragm tanks have been widely used, but the trend seems to be away from that type of tank. This implies that filling gaps in the knowledge base for such configurations should have a lower priority unless there is an indication that these tanks will return to wider favor.

Although better analytical models are sorely needed, this study uncovered no obvious new approaches. The data that is presented here, however, provides truth models for testing analytical methods that may be developed in the future. It is clear from the complexity of the behavior covered by this study that to be considered reliable, any analytical model will probably have to be "tweaked" to match existing flight and test data.

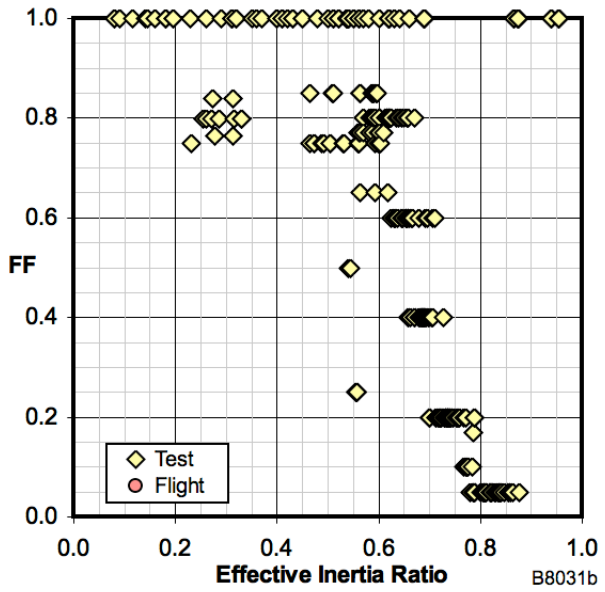

Figure 13-1 Parameters Covered for Centerline Spherical Tanks (No Diaphragms)

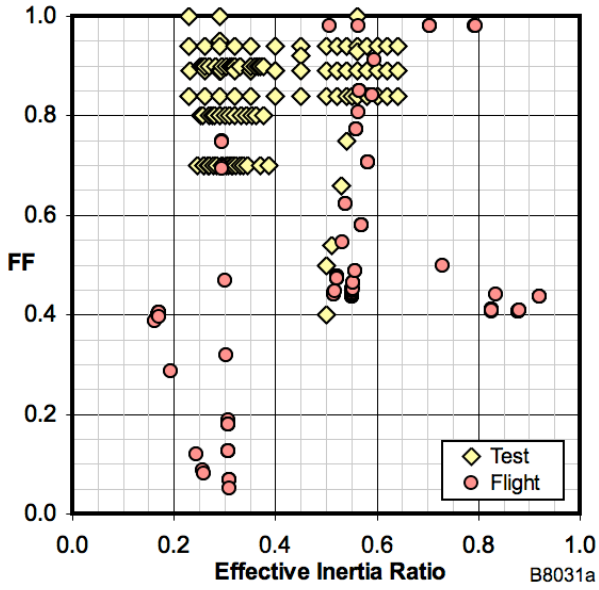

Figure 13-2 Parameters Covered for Off-Axis Spherical Tanks (No Diaphragms)

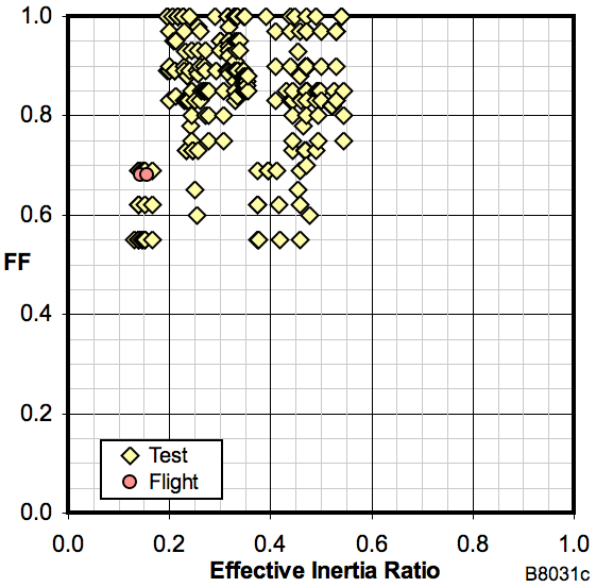

Figure 13-3 Parameters Covered for Centerline Tanks with Cylindrical Sections, Hemispherical Ends, and No Diaphragms

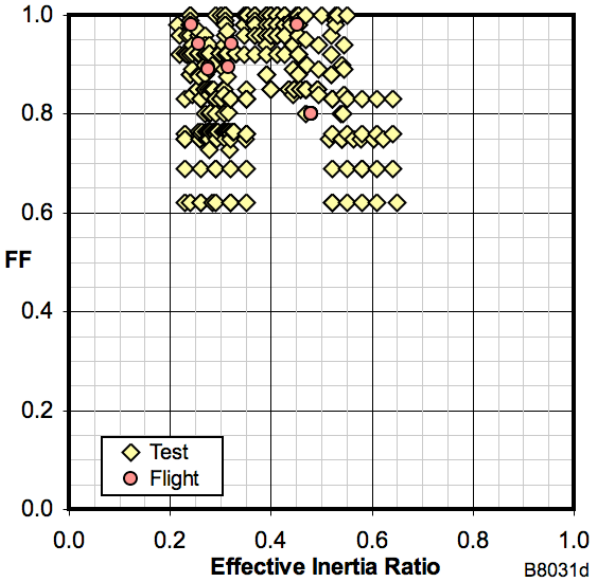

Figure 13-4 Parameters Covered for Off-Axis Tanks with Cylindrical Sections, Hemispherical Ends, and No Diaphragms

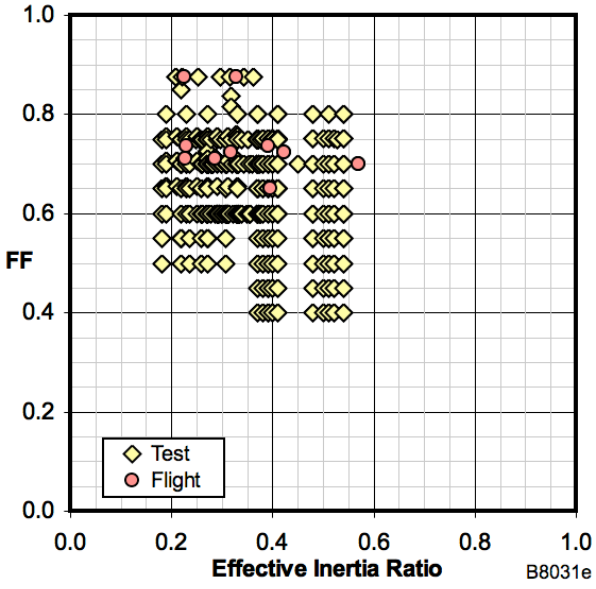

Figure 13-5 Parameters Covered for Centerline Diaphragm Tanks

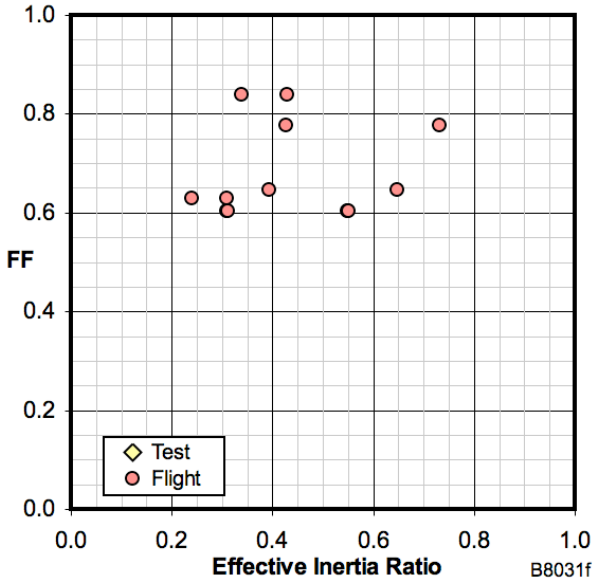

Figure 13-6 Parameters Covered for Off-Axis Diaphragm Tanks

14. Summary of Propellant Tank Influences

The following is a brief summary of known behavior of propellant tanks that have flown on spinning space vehicles or been subject to spinning ground test.

14.1 Non-Diaphragm Tanks

Spherical tanks have extensive flight and test history. [redacted] Liquid/nutation resonances have not been observed in off-axis spherical tanks. Energy dissipation in off-axis spheres is dominated by flow past internal hardware and the dissipation rate tends to increase with fill fraction, with the maximum dissipation rate often occurring when the tank is 100% full.

Spheroidal tanks have only a limited test and flight history. Tests have shown that even small deviations from spherical can greatly increase energy dissipation, although indications are that prolate tanks are much worse than oblate ones. [redacted]

Sphere-cone or "conisphere" tanks have extensive flight and test history and have been shown to be subject to severe inertial wave resonances at many combinations of fill fraction and inertia ratio. This is probably the most extensively tested tank configuration, but the data is largely proprietary and was unavailable for this study. Although this tank shape saw frequent use two decades ago, there is no indication that propulsion system designers plan to use it in the future.

Cylindrical tanks have been extensively studied, although the focus has been largely on spinning artillery shells in which the tank's symmetry axis is coincident with the spin axis. In this context, severe liquid/nutation resonances have been identified in partially filled and completely filled tanks. This author is aware of only one use of a nearly cylindrical tank on a space vehicle, and that configuration had the tank's symmetry axis perpendicular to the spin axis. Test and flight performance showed that particular configuration to be relatively benign.

Cylindrical tanks with hemispherical ends have seen regular use on spinning space vehicles during the last 15 years and have thus been subject to a variety of test programs. Experience is limited to tanks with the symmetry axis parallel to the vehicle's spin axis. Liquid/nutation resonances have been observed in both on-axis and off-axis tanks, including completely filled tanks. [redacted]

[redacted]

Hemispherical tank tests on an air bearing have shown strong liquid/nutation resonances for a fill fraction of 1.0. Although this tank shape is unlikely to see application on a space vehicle, the test results reinforce the observation that non-spherical tanks are susceptible to vigorous subsurface flow.

It is essential to recognize that tank shape is only one of many characteristics that must be considered when evaluating the influence of contained liquids on nutation performance. In particular, the configuration of internal hardware (baffles, sumps, drain tubes, surface tension vanes, etc.) can have a profound effect on vehicle behavior.

14.2 Tanks with Diaphragms or Bladders

Tanks with diaphragms or bladders can be more sensitive to fill fraction than other tanks because the liquid is within a partially flexible container whose shape is a function of both fill level and initial conditions. Drop tests have shown strong sensitivity to diaphragm equilibrium shape, although the characteristics and full magnitude of the sensitivity has been only partially mapped out. Liquid/nutation resonance has been observed in at least one bladder tank.

14.3 Baffles

[redacted]

14.4 General Observations

Care should be taken in applying the data in this report to new configurations. This is especially true for non-diaphragm tanks because it seems that nearly every tank uses a different propellant management device, even if it is designed by the same organization for a tank with dimensions nearly identical to one that flew before. Tests have shown that nutation performance can be very sensitive to PMD shape, dimensions, and flexibility. Available data suggests that internal hardware tends to increase the dimensionless time constant for operations near a liquid/nutation resonance and decreases the DTC for operations away from resonance. In other words, for a minor axis spinner, internal hardware tends to improve performance at or near resonance but tends to degrade performance away from resonance. Test data also indicates that PMD flexibility reduces its influence on nutation performance.

15. References

Agrawal, 1982, "Stability of Spinning Spacecraft with Partially Liquid-Filled Tanks," *Journal of Guidance, Control, and Dynamics,* Vol. 5, No. 4, pp. 344-350.Agrawal, 1984, "An Overview of Intelsat Activities on Liquid Slosh," Proceedings of the First INTELSAT/ESA Symposium on the Dynamic Effects of Liquids on Spacecraft Attitude Control, pp. 99-120.

Agrawal, 1993, "Dynamic Characteristics of Liquid Motion in Partially Filled Tanks of a Spinning Spacecraft," *Journal of Guidance, Control, and Dynamics* Vol. 16, No. 4, pp. 636-640.

Agrawal and James, 1981, "Energy Dissipation Due to Liquid Slosh in Spinning Spacecraft," 3rd VIP&SU/AIAA Symposium on Dynamics and Control of Large Flexible Structures, AIAA-83-4512, pp. 439-452.

Alfriend, 1974, "Partially Filled Viscous Ring Nutation Damper," *Journal of Spacecraft and Rockets,* Vol. 11, No. 7, 456-462.

Cartwright, Massingill, and Trueblood, 1963, "Circular Constraint Nutation Damper," *AIAA Journal,* Vol. 1, No. 6, pp. 1375-1380.

D'Amico, 1974, "Stability of Satellites and Unusual Aerodynamic Shaped Vehicles Carrying Liquid Payloads," BRL-MRT-2392, US Army Ballistic Research Labs, Aberdeen, MD.

Deffenbaugh, Dodge, and Green, 1998, "Final Report for the Liquid Motion in a Rotating Tank Experiment (LME)," Southwest Research Instititute Report SwRI 6322-FNL-01.

Dodge, 1994, "Propellant Dynamics and PMD Design for the Near Earth Asteroid Rendezvous (NEAR) Spacecraft," Final Report of Project 04-6297, Southwest Research Institute, San Antonio, TX.

Garg, Furumoto, and Vanyo, 1986, "Spacecraft Nutational Instability Prediction by Energy Dissipation Measurements," *Journal of Guidance, Control, and Dynamics,* Vol. 9, No. 3, pp. 357-362.

Green, Burkey, Dodge, and Walter, 2002, "Nutation Time Constant Model Parameters for the CONTOUR Spacecraft," Final Report of Project 18.04617, Southwest Research Institute, San Antonio, TX

Green and Burkey, 2007, "Nutation Time Constant Model Parameters for the SSTR On-Axis Configuration (Deep Impact/Pluto New Horizons Spacecraft)," Final Report of Project 18.12441, Southwest Research Institute, San Antonio, TX

Greenspan, 1969, *The Theory of Rotating Fluids,* Cambridge University Press.

Guibert, 1986, "Forced Motion on Spinning Test for Slosh-Moment Investigations," Institut von Karman de Dynamique des Fluides and ESA Symposium on Fluid Dynamics and Space, Rhodes-Saint-Genese, Belgium, ONERA, TP 1986-82.

Guibert, 1987, "A Free-Fall Facility to Investigate Liquid Slosh Effects on Spinning Spacecraft," *Space Communications and Broadcasting,* Vol. 5, No. 4, pp. 281-291.

Harrison, 1984, "A Review of the Scale Model Drop test Method for Predicting Spacecraft Nutation Divergence," Proceedings of the First INTELSAT/ESA Symposium on the Dynamic Effects of Liquids on Spacecraft Attitude Control, pp. 295-305.

Harrison, 1987, "Analysis of Spacecraft Nutation Dynamics Using the Drop Test Methods," *Space Communications and Broadcasting,* Vol. 5, No. 4, pp. 265-280.

Harrison, Garg, and Furumoto, 1983, "A Free-Fall Technique to Measure Nutation Divergence, and Applications," AAS/AIAA Astrodynamics Conf., AAS 83-372, pp. 685-702.

Hubert, 2000, "Surface Tension Lockup in the IMAGE and Lunar Prospector Nutation Dampers," Hubert Astronautics Technical Report B0031, NASA/GSFC Contract S-39986-G.

Hubert and Goodzeit, 1983, "The Effects of Propellant Motion on a Spinning Satellite with Vaned Tanks," AIAA Guidance & Control Conference, Gatlinburg, Tenn., AIAA 83-2262.

Hubert, Shaw, and Berg, 1988, "Computer-Aided Stability Analysis of Spinning Spacecraft with On-Board Liquids," AIAA Astrodynamics Conference, AIAA 88-4314,

Hubert and Swanson, 2001, "Surface Tension Lockup in the IMAGE Nutation Damper – Anomaly and Recovery," NASA GSFC Flight Mechanics Symposium.

Kana and Dodge, 1979, "Preliminary Study of Liquid Slosh in the Tracking and Data Relay Satellite Hydrazine Tanks," Final Report of Project 02-5887, Southwest Research Institute, San Antonio, TX.

Kana and Dodge, 1981, "Study of Liquid Slosh in the Tracking and Data Relay Satellite Hydrazine Tanks," NASA Contractor Report, NASA CR-166745.

Kreis, Kurz, Klein, and Deloo, 1996, "Static and Dynamic Modeling of Diaphragm Tanks", Proceedings of the ESA International Conference on Spacecraft Structures, Materials and Mechanical Testing, Noordwijk, Netherlands, pp. 845-852.

Marcè, Torres, Assemat, and Michel, 1981, "Energy Dissipation in EXOSAT Tanks: Test Results," CNES Technical Note CNES-NT-99.

Martin, 1971a, "Experimental Investigations on the Fuel Slosh of Dual-Spin Spacecraft," *Comsat Technical Review,* Vol. 1, No. 1, pp. 1-20.

Martin, 1971b, "Fuel Slosh and Dynamic Stability of Intelsat IV," AIAA Guidance, Control, and Flight Mechanics Conference, Hempstead, NY, AIAA 71-954.

McIntyre, 1984, "Spacecraft/Fluid Interaction Program at Hughes Aircraft Co.," Proceedings of the First INTELSAT/ESA Symposium on the Dynamic Effects of Liquids on Spacecraft Attitude Control, Washington, DC, pp. 199-227.

McIntyre and McIntyre, 1982, "Some Effects of Propellant Motion on the Performance of Spinning Satellites," *Acta Astronautica,* Vol. 9, No. 11, pp. 645-661.

McIntyre and Miyagi, 1976, "A General Stability Principle for Spinning Flexible Bodies with Application to the Propellant Migration – Wobble Amplification Effect," Dynamics and Control of Non-Rigid Spacecraft Symposium, Frascati, Italy.

McIntyre and Tanner, 1987, "Fuel Slosh in a Spinning On-Axis Propellant Tank: An Eigenmode Approach," *Space Communications and Broadcasting,* Vol. 5, No. 4, pp. 229-251.

Mingori and Harrison, 1974, "Circularly Constrained Particle Motion in Spinning and Coning Bodies," *AIAA Journal,* Vol. 12, No. 11, pp. 1553-1558.

Nayfeh and Meirovitch, 1974, "The Stability of Motion of Satellites with Cavities Partially Filled With Liquid," AIAA Aerospace Sciences Meeting, Washington, DC.

Neer and Salvatore, 1972, "Fuel Slosh Energy Dissipation on a Spinning Body," Hughes Aircraft Report SCG 20047R.

O'Hern, Baddeley, and Rekowski, 1972, "Analysis of Effects of Fluid Energy Dissipation on Spinning Satellite Control Dynamics," AIAA Guidance and Control Conference, Stanford California, AIAA 72-886.

Pawlowski and Imbert, 1984, "Advanced Devices for Measurement of Energy Dissipation in Rotating Tanks," Proceedings of the First INTELSAT/ESA Symposium on the Dynamic Effects of Liquids on Spacecraft Attitude Control, Washington, DC, pp. 55-73.

Peterson, 1976, "Air Bearing Spin Facility for Measuring Energy Dissipation," NASA Technical Note, NASA TN D-8346.

Pocha, 1984, "Experimental and Analytic Investigation of Spacecraft Nutation Dynamics," Proceedings of the First INTELSAT/ESA Symposium on the Dynamic Effects of Liquids on Spacecraft Attitude Control, Washington, DC, pp. 367-391.

Pocha, 1987, "An Experimental Investigation of Spacecraft Sloshing," *Space Communications and Broadcasting,* Vol. 5, No. 4, pp. 323-332.

Pocha, 1995, "An Experimental Verification of the Stability Theory For Spinning Fluid-Filled Spacecraft," *Space Communications,* Vol. 13, No. 4, pp. 289-297.

Quadrelli, 2005, "Modeling and Analysis for Nutation Time Constant Determination of On-Axis Diaphragm Tanks on Spinners: Application to the Deep Space One Spacecraft," *Journal of Spacecraft and Rockets, Vol. 42, No. 3, pp. 530-542*.

Reiter and Lee, 1966, "Zero Gravity Stability Testing of a Liquid-Filled Space Vehicle," *Chemical Engineering Progress Symposium Series,* Vol. 62, No. 61, pp. 178-183.

Scott and D'Amico, 1973, "Amplitude-Dependent Behaviour of a Liquid-Filled Gyroscope," *Journal of Fluid Mechanics,* Vol. 60, No. 4, pp. 751-758.

Selmi and Herbert, 1995, "Resonance Phenomena in Viscous Fluids Inside Partially Filled Spinning and Nutating Cylinders," *Physics of Fluids,* Vol. 7, No. 1, pp. 108-120.

Slabinski, 1978, "Intelsat IV In-Orbit Liquid Slosh Tests and Problems in the Theoretical Analysis of the Data," *Comsat Technical Review,* Vol. 8, No. 1, pp. 1-40.

Stofan and Summer, 1963, "Experimental Investigation of the Slosh-Damping Effectiveness of Positive Expulsion Bags and Diaphragms in Spherical Tanks," NASA Technical Note, TN D-1712.

Vanyo, 1973, "An Energy Assessment for Liquids in a Filled Precessing Spherical Cavity," *Journal of Applied Mechanics,* Vol 40, No. 4, pp. 851-856.

Vanyo, 1984, "Fluid Velocities and Energy Dissipation: Experiments," Proceedings of the First INTELSAT/ESA Symposium on the Dynamic Effects of Liquids on Spacecraft Attitude Control, Washington, DC, pp. 75-97.

Vanyo and Likins, 1971, "Measurement of Energy Dissipation in a Liquid-Filled, Precessing, Spherical Cavity," *Transactions of the ASME,* pp. 674-682.

Vanyo and Likins, 1973, "Use of Baffles to Suppress Energy Dissipation in Liquid-Filled Precessing Cavities," *Journal of Spacecraft and Rockets,* Vol. 10, No. 10, pp. 627-628.

Wilde, 1997, "A Cost-Effective Means to Predict the Nutational Stability Time Constant of Spin-Stabilized Spacecraft," AIAA Guidance, Navigation, & Control Conference, AIAA 97-3619.

Zedd and Dodge, 1984, "Energy Dissipation of Liquids in Nutating Spherical Tanks Measured by a Forced Motion Spin Table," AIAA Guidance, Navigation, & Control Conference, Seattle, WA, AIAA 84-1842.

Zedd and Dodge, 1985, "Energy Dissipation of Liquids in Nutating Spherical Tanks Measured by a Forced Motion Spin Table," Naval Research Laboratory Report NRL-8932.

16. Glossary

ANC – Active nutation control

Apparent inertia ratio – The inertia ratio of an inertially symmetric rigid body that has the same nutation frequency as a vehicle with mobile onboard liquid when both are spinning at the same rate. In this report, the *apparent inertia ratio* is based on measured spin rate and measured nutation frequency. *[See effective inertia ratio.]*

Aspect ratio – The length of a tank divided by its diameter.

Bladder – A flexible inner container that separates a liquid propellant from the pressurant gas. In a bladder tank, the rigid outer walls are not wetted. *[See diaphragm.]*

Bond number – The ratio of inertial force (i.e., gravitational or acceleration force) to surface tension force, usually represented by the symbol N_B. The significance of specific Bond numbers and ranges of Bond numbers is as follows:

Bond Number	Significance
$N_B < 1$	Surface tension has a dominant effect on liquid motion.
$N_B = 0.843$	The critical value for bubble migration in a tube. If the Bond number is below this value, a bubble in contact with a tube wall will not move.
$N_B = 1.0$	Surface tension and inertial forces are of equal magnitude.
$1 < N_B < 10$	Surface tension has a significant effect on liquid motion and must be considered.
$10 < N_B < 100$	Surface tension has some effect on liquid motion and may need to be considered.
$N_B > 100$	Surface tension can usually be ignored.

Diaphragm – A flexible barrier that separates a liquid propellant from the pressurant gas. The contained liquid is in direct contact with both the flexible barrier and the portion of the tank's rigid outer wall that is on the propellant side of the diaphragm. *[See bladder.]*

DTC – Dimensionless Time Constant. See Section 5.1 for details.

Effective inertia ratio – The inertia ratio of an inertially symmetric body with the same nutation frequency as the real vehicle when both are spinning at the same rate. In this document, the *effective inertia ratio* is based on calculated moments of inertia and assumes that any onboard liquids are frozen in their nominal locations. *[See apparent inertia ratio.]*

FF – Fill fraction.

Fill fraction – The fraction of a tank's total volume that is occupied by liquid. Note that by this definition a fill fraction of 1.0 may exceed the tank's useful capacity.

Froude number – In a ground-based system, this is the ratio of centrifugal force to gravitational force. In flight, it is the ratio of centrifugal acceleration to thrust-induced acceleration. The Froude number is essentially infinite during non-thrusting operations in space.

ID – Internal diameter.

Inertially asymmetric – A vehicle is considered to be inertially asymmetric if the principal axes perpendicular to the spin axis have unequal moments of inertia.

Inertially symmetric – A vehicle is considered to be inertially symmetric if the principal axes perpendicular to the spin axis have identical moments of inertia. An inertially symmetric vehicle is dynamically equivalent to a homogeneous cylinder.

Inertia ratio – The ratio of a vehicle's moment of inertia about it's nominal spin axis (a principal axis) to a principal moment of inertia about an axis perpendicular to the spin axis. If the vehicle is inertially asymmetric, the ratio is often defined as the value that is closest to 1.0. *[See effective inertia ratio and apparent inertia ratio.]*

Intermediate axis – On a vehicle with three unequal principal moments of inertia, the intermediate axis is the principal axis that is neither the major axis nor the minor axis.

IR – Inertia ratio.

Major axis – The principal axis with the maximum moment of inertia.

Major axis spinner – A vehicle that is designed to spin about its major axis.

Minor axis – The principal axis with the minimum moment of inertia.

Minor axis spinner – A vehicle that is designed to spin about its minor axis.

Nutation – A deviation from simple spin about a principal axis that is characterized by cyclic body rates. An example is the wobbling motion of a poorly thrown football.

Nutation angle – The angle between the nominal spin axis (a principal axis) and the vehicle's angular momentum vector. For an inertially asymmetric vehicle, this angle varies at twice the nutation frequency.

Nutation frequency – The frequency at which transverse body rates vary during nutation. See Section 2.1.1 for a mathematical definition.

Nutation synchronous mode – A condition in which liquid in a partially filled centerline tank has a unidirectional circulation about the spin axis at the nutation rate. Sometimes referred to as "rotary slosh".

NTC – Nutation time constant

PMD – Propellant management device.

Post-burn – Refers to the configuration of a spacecraft/upper stage stack after burnout of the spinning solid upper stage.

Pre-burn – Refers to the configuration of a spacecraft/upper stage stack before ignition of the spinning solid upper stage.

Rotary slosh mode – A condition in which liquid in a partially filled centerline tank has a unidirectional circulation about the spin axis at the nutation rate. Usually referred to as the "nutation synchronous mode".

Spin axis – The vehicle's nominal axis of rotation.

Time constant – The time required for an exponentially growing or exponentially decaying parameter to change in magnitude by a factor of e, where $e = 2.71828\ldots$ For spinning vehicles, "time constant" usually refers to nutation growth or decay. In this report, positive time constants indicate growth and negative time constants indicate decay.

Transverse axis – An axis that is perpendicular to the vehicle's spin axis and that passes through the center of mass. Often refers to a principal axis.

17. Index of NASA Missions Covered in This Report